DELFT UNIVERSITY OF TECHNOLOGY

REPORT 04-04

Numerical modeling of optical phase-change recording

J.H. Brusche

ISSN 1389-6520

Reports of the Department of Applied Mathematical Analysis

Delft 2004

Numerical modeling of optical phase-change recording

J.H. Brusche[1]

September 17, 2004

[1]Delft University of Technology, Faculty of Electrical Engineering, Mathematics and Computer Science, Department of Applied Mathematical Analysis, P.O. Box 5031, 2600 GA Delft, The Netherlands, phone: 31 15 2787608, fax: 31 15 2787209 (j.h.brusche@ewi.tudelft.nl)

Contents

Chapter 1

Introduction

Research and development on the subject of phase-change optical recording has become more and more important, especially since rewritable optical data storage media have acquired a solid position in the consumer market. In this report we present the results of a literature study concerning the (numerical) modeling of phase-change optical recording. This literature study has been performed as part of a PhD-research project which aims at robustly and accurately modeling the writing and erasing of data in rewritable optical disks.

The contents of this report can be outlined as follows. In Chapter 2 the basics of phase-change optical recording are explained in detail. The main goals of this chapter are to first of all try to provide a satisfying answer to the question: 'Really, how does it work?' and secondly make the reader acquainted with the terminalogy.

Then, in Chapter 3, the modeling of the phase-change recording process is considered. The optical, thermal and materials science aspects are discussed successively. Specific attention is given to the modeling details concerning (re)crystallization, a process which plays a significant role during the erasure of data.

The writing of data can be modeled as a two-phase moving boundary problem. Since only for a select number of this type of problems can be solved analytically, numerical methods are the only alternative. In Chapter 4 a survey of numerical methods for phase-change problems is presented. The level set and enthalpy approaches will be discussed in detail. Based on a method comparison we give a recommendation to which method is most suitable for solving the two-phase moving boundary problem related to optical rewritable recording.

Chapter 2

An introduction to phase-change recording

Since the introduction of the audio CD in 1983, optical storage media have started to dominate the portable data storage market. In this chapter we will consider the recordable version of the CD and its successors, in particular the rewritable disks. The main advantage of these rewritable disks is that data can be written and erased many times. This is achieved by using a so called phase-change material, which by means of heating with a laser beam can (locally) be changed very quickly from a crystalline to an amorphous state, and vice versa. We will consider the various aspects of the phase-change recording process in more detail in Sections 2.2-2.5. In the concluding section of this chapter we will discuss some possibilities for capacity and speed improvements and some known limitations and problems in high density recording.

2.1 A brief history of optical recording

After the enormous success of the CD(-ROM), a growing consumer demand for recordable optical storage media was eventually answered in 1990 with the introduction of the CD-Recordable (CD-R). With its storage capacity of 650 Megabytes (MB), equal to that of the CD(-ROM), it enabled people to make backup copies or to create their own data.

In 1997 the limitation of recording only once was overcome by the introduction of the CD-rewritable (CD-RW), allowing rewriting up to a thousand times. In the same year, a race between manufactures focused on larger data capacity and transfer rates, initiated earlier by the forthcoming of high quality MPEG-2 encoded video material and the increased data traffic over the

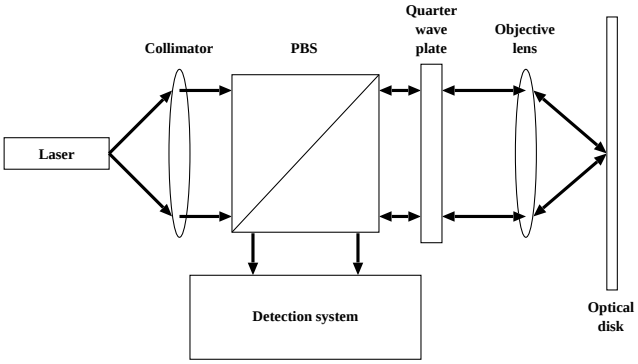

Figure 2.1: Setup for an optical system.

Internet, eventually resulted in the introduction of the digital versatile disk (DVD). Its storage capacity of 4.7 Gigabytes (GB) and even 8.5 GB for the dual layered version, in combination with a maximum data transfer rate of 11.2 megabits per second (Mb/s), easily fulfilled the newly imposed demands. The possibility to play CD's with the DVD-players and the rapidly growing amount of film titles that became available, made that the popularity growth of the DVD even surpassed that of the CD.

Besides the read-only DVD, the DVD+R, for single time recording, and more recently the DVD+RW, for multiple writing, and the DVD random access memory (DVD-RAM), have been introduced to the general public.

The latest medium in the race for storage capacity and speed among (re)writable storage media, is the Blu-ray disk (BD) (the former digital video recording disk (DVR) standard), developed within the framework of high-definition television (HDTV) by Philips and Sony around 1999. A single layer BD disk has a storage capacity of 23.5GB or 25GB, while the capacity of the double layer version is aimed at a dazzling 47GB or 50GB. For instance see [9], pp. 99-101.

2.2 The optical system

The various data storage disks mentioned in the previous section all have in common that the reading, and if applicable writing, of data on the disk is done optically. For both reading and writing, the same optical system is used, but with different power levels of the laser beam.

In Figure 2.1 the setup of an optical head of an optical system is shown. The optical head contains a laser diode, a collimating lens, a polarizing beam splitter (PBS), a quarter wave plate, an objective lens and the detection sys-

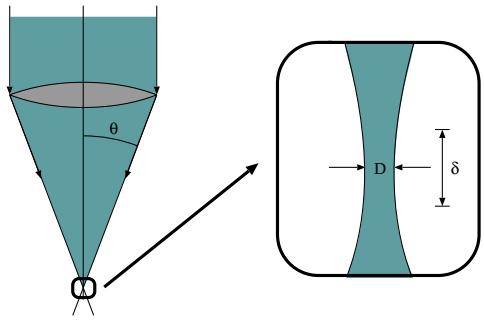

Figure 2.2: The NA of a lens is given by $\sin(\theta)$.

tem. The collimating lens is used to collimate the diverging linearly polarized beam emitted by the laser diode. After passing through the PBS, the light incident on the quarter wave plate is circularly polarized. Finally, the objective lens focuses the beam on the optical disk.

The light that is reflected by the metallic layer of the disk is collimated by the objective lens on its way back through the optical system. The quarter wave plate then converts the dominantly circularly polarized reflected light into a linear polarized beam such that the polarization is perpendicular to that of the incident beam. The PBS finally redirects the reflected beam onto the detection system. During the readout of data, the detection system can determine whether a 'zero' or a 'one' is read, based on a priori knowledge about the differences between the reflected intensities when the spot is focused on a pit or a non pit (for pre-recorded disks), on a decomposed or intact dye material (for write once media) or on the amorphous or crystalline state of phase-change material (for rewritable media). See [9], pp. 101-102.

Read-only disks such as the CD(-ROM) and the DVD are pressed. The pits (and non pits) that represent the binary data are positioned on a concentric, outwards spiraling track. In order to correctly read from these optical disks, the focused spot must be kept centered on this track. When the optical head moves away from the track's center, an asymmetry in the reflected field is induced. Whenever such an asymmetry is detected, the optical head is guided such that the beam is again focused on the center of a track. This procedure is called tracking.

In addition to the read-out of data, recordable and rewritable systems use tracking during writing. But, in absence of reference points in sections of the disk where no data has been recorded, tracking is not possible. To that purpose, the surface of these disks contains a concentric, outwards spiraling groove. Therefore, in radial direction, the disk is said to have a (periodic) 'land and groove' structure.

The dimensions of the grooves as well as the size of the amorphous regions (marks) that represent the binary data, are in the order of the wavelength of the incident light. The geometrical assumption that a parallel beam that is incident on a positive lens converges into a single point, is then no longer applicable. Due to diffraction by the finite aperture of the lens, the diameter of a focused spot is given by [22]:

$$D \approx \frac{\lambda}{\mathrm{NA}}. \tag{2.1}$$

In formula (2.1), λ is the wavelength of the incident light and NA is the numerical aperture of the objective lens. The NA is the sine of the angle between the outer ray and the principle axis of the objective lens. The focal depth (or depth of focus) δ of a spot, can be defined as the range (in image space) over which the focused spot diameter remains below an arbitrary limit, see Figure 2.2. In an imaging system the depth of focus would be the distance (in object space) over which the system delivers a sharp image. The focal depth is given by:

$$\delta \approx \frac{\lambda}{\mathrm{NA}^2}. \tag{2.2}$$

An overview of the specific values of the optical and mechanical parameters mentioned in this section is listed in Table 2.1 for the various optical recording disks.

2.3 The principle of phase-change recording

In systems for rewritable disks, the active layer of the optical disk is subject to crystallographic changes upon heating by laser radiation [17]. By applying short high-power laser pulses that melt the crystalline phase-change material

Table 2.1: An overview of several optical and mechanical properties of the recordable and rewritable media. The values given for the track pitch (TP) and the thickness of the recording stack (Δ) are average values. The specified wavelengths are in air.

medium	capacity [GB]	λ [nm]	NA [-]	D [nm]	TP [nm]	δ [nm]	Δ [nm]
CD(-R/-RW)	0.65	780	0.50	1560	1500	3120	≈ 250
DVD(-R/+RW)	4.7	650	0.65	1000	740	≈ 1540	≈ 250
BD	23.5/25	405	0.85	≈ 470	320	≈ 550	≈ 150

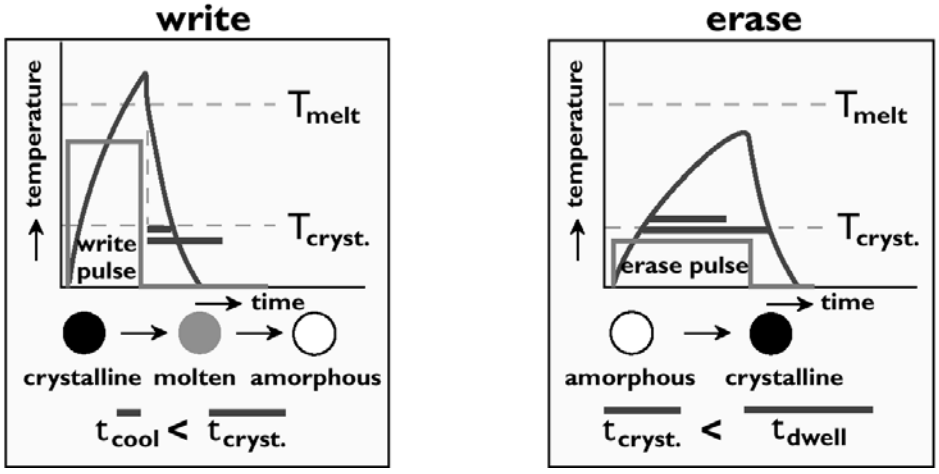

Figure 2.3: The write and erase process illustrated.

(temperature $T > T_{melt}$), followed by quenching to temperatures below the crystallization temperature T_{cryst}, amorphous marks are written, see Figure 2.3. In the context of optical recording the crystallization time can be defined as the time required for an amorphous region to fully regain the crystalline state. The quenching procedure prevents the nucleation and growth of the crystalline phase during the cooling down ($t_{cool} < t_{cryst}$).

Marks are erased by heating the amorphous material to a temperature between its melting temperature T_{melt} and its crystallization temperature T_{cryst} for a time t_{dwell} during which the spot remains above the amorphous region. In order to erase the complete mark, i.e. for the whole amorphous region to regain the crystalline state, t_{dwell} should be longer than the crystallization time of the phase-change material ($t_{dwell} > t_{cryst}$). The crystallization time is thus taken to be the time required to completely erase the mark. The speed at which data can be written is therefore strongly dependent on the type of material used in the active layer.

Two kinds of phase-change materials exist, namely nucleation dominated and crystal growth-dominated. In the former, small crystalline nuclei inside the amorphous mark start to grow until they impinge upon each other. In the latter, the probability of the occurrence of crystal nuclei is low but crystal growth is very fast. The crystallization of the amorphous mark is then largely due to the inward growth of the boundary between the mark and the crystalline surrounding.

The most commonly used phase-change materials are stoichiometric SbTe alloys, in particular Ge-Sb-Te [44] and Ag-In-Sb-Te [26]. Due to relatively high crystallization times (t_{cryst} = 100-250 ns), Ag-In-Sb-Te alloys are mainly

used in low speed applications such as CD-RW. The various compositions of this alloy allow rewriting between a thousand and ten thousand times. For applications in high-speed recording, such as DVD+RW, Ge-Sb-Te alloys are used ($t_{cryst} < 50$ ns). The rewritability of these types of compositions ranges between 10^5 and 10^6 times. Recently, doped eutectic[1] SbTe alloys have been proposed for the Blu-ray disk system [4] and issues like their stability and cyclability have been addressed [5].

The reading of written information is done by measuring intensity modulations of the light reflected by the disks. In order to be able to distinct between both phases, the contrast between the reflectivity of the crystalline and the amorphous state should be high.

2.4 The structure of a PC-disk

Optical rewritable disks can contain either one or two recording layers. For single-layered phase-change disks the so-called recording stack usually consists of four different layers. In Figure 2.4 the recording stack for a typical Blu-ray disk has been illustrated. The recording stack configuration shown in the figure is called an IPIM stack [17]. The various layers of the IPIM-stack are sputtered on a pre-grooved substrate. On top of the substrate, made of poly-carbonate or glass, is a dielectric **I**nterference layer. On top of this dielectric layer there are subsequently the **P**hase-change layer, another dielectric **I**nterference layer and a metallic **M**irror layer.

The dielectric layers, generally a mixture of ZnS and SiO_2, and the metallic layer, made of Al or Au, protect the phase-change layer from environmental influences. In addition, their thickness is chosen such that they optimize the optical contrast between the crystalline and amorphous state. The dielectric layer between the phase-change layer and the substrate is relatively thick in order to protect the substrate from thermal damage during writing. The dielectric layer between the phase-change layer and the metallic layer is relatively thin such that sufficient heat can reach the metallic layer to make quenching possible. During quenching the metallic layer acts as a heat sink and is taken sufficiently thick for this purpose. Apart from the chemical composition of the IPIM-layers and their thickness, the characteristics of the interfaces are also of great importance. Chemical reactions between layers could influence the performance of the disk. We refer to Table 2.1 for an overview of the approximate thickness of the recording stack, denoted as Δ, for the various recordable media.

[1] a mixture of substances having a minimum melting point

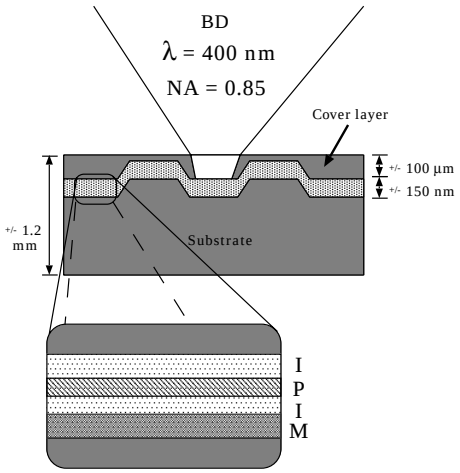

Figure 2.4: An illustration of the stack for the Blu-ray disk, with an IPIM recording stack. The recording stack is placed relatively close to the disks surface in order to preserve a small spot diameter. The thickness of the layers are not to scale.

Besides the optical and thermal properties mentioned, the layers must consist of materials of mechanically good quality to avoid or delay the appearance of defects, e.g. pinholes and micro-cracks. These defects are induced by material flow and thermal deformation during repeated heating and quenching.

Dual-layered stacks, which allow for an increase in data capacity, have been proposed for the Blu-ray disk system [41]. The two recording stacks are optically accessed from one side of the disk, see Figure 2.5. In order to ensure that a sufficient amount of light can reach the second recording stack L1, there is a practical requirement of 50% transparency for the first recording stack L0. As a result, a conventional non-transparent metal layer can not be used in L0. As a result of the omission of a metal layer in the first recording stack, a slow cooling behavior is observed in L0. Several improvements have been proposed to improve the thermal behavior of L0 stacks such as additional transparent heat sinks [41] or thin semi-transparent metal layers, such as silver alloys [1]. A drawback of these solutions is the decrease of sensitivity of the stack with respect to write power.

It is not surprising that in dual-layered stacks, thermal interference between the recording stacks needs to be avoided. This is achieved by taking the the so-called spacer layer, that separates both recording stacks, thick enough. As a result, the thermal behavior of the two stacks can be studied independently.

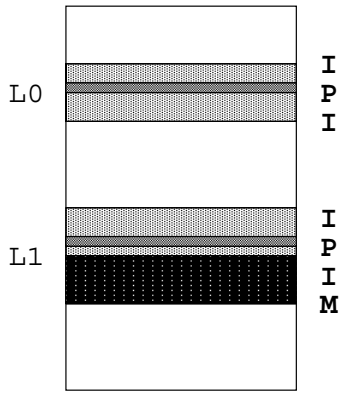

Figure 2.5: Sketch of the dual-stack phase-change disk. L0 is the first recording stack, L2 is the deep recording stack. Both recording stacks are optically accessed from the top side. The thickness of the different layers are not to scale.

For both single-layered as dual-layered stacks other configurations have been and are still researched. However, in this literature survey such stack configurations will be kept out of consideration.

2.5 Recording strategies

Several methods have been proposed for writing data on rewritable disks. In the early nineties, recording strategies such as 'pulse position' recording and 'mark edge' recording have been studied. When 'pulse position' recording is used, all amorphous marks have the same length. As a consequence, the system can only read information out of the spaces between the written marks.

With 'mark edge' (or 'pulse-width') recording, the written marks vary in length, which allows for information to be read from both the length of the amorphous marks as well as the length of the crystalline spaces between the marks. During the writing of each mark, the power of the spot is kept at a constant high power level. A serious drawback of this strategy is that due to accumulation of heat during melting the recorded mark tends to have a teardrop shaped distortion.

In order to avoid the occurrence of this unwanted effect, 'multi pulse' recording is used. With this recording technique each mark is formed by a train of successive short high-power laser pulses generating overlapping amorphous dots as shown in Figure 2.6. In between the pulses, the laser power is set to a low level, so that after each laser pulse the molten material

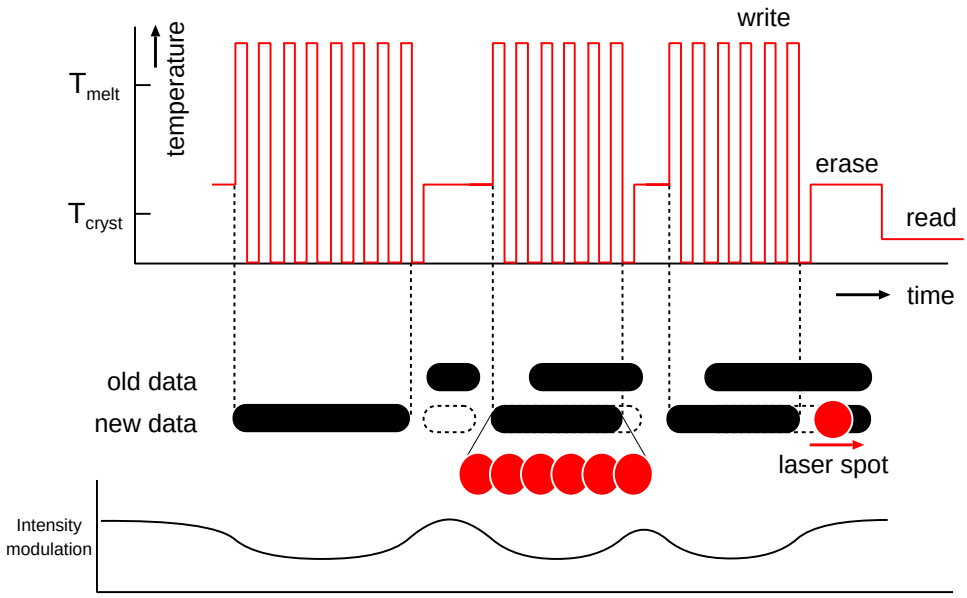

Figure 2.6: The direct overwrite strategy. The intensity of the high-power laser is set to such a level that during the recording of new data, existing old data is erased. During reading, modulations in the intensity of the reflected light can be measured.

is quenched and the accumulation of heat is avoided. When no marks are written the laser power is switched to an intensity level which is high enough to crystallize the material and erase possible earlier written marks. Since this method of multi-pulse recording enables the system to overwrite old marks directly, it is called a direct overwrite (DOW) method.

The most commonly used schemes for writing the amorphous marks are 'groove' recording and 'land-groove' recording. In case of groove recording, the marks are only written in the grooves of the disk. When the land-groove scheme is used, the marks are also written in the lands. The distance between adjacent grooves is called the groove pitch and the distance between adjacent tracks is called the track pitch. Thus, for groove recording the track pitch and groove pitch are equal, whereas in case of land-groove recording, the groove pitch is twice the track pitch.

2.6 Some remarks on high density recording

As has been mentioned in Section 2.1, research and development in the field of recordable and rewritable disks is concentrated on both the increase of

data storage capacity as well as data transfer rates. An increase of capacity (or bit density) can be realized by either reducing the track pitch, i.e. the radial density, or using smaller mark lengths (linear density). The average mark length depends on the wavelength λ of the laser light and the numerical aperture of the objective lens. By reducing the spot diameter D as defined by (2.1), smaller marks can be written and detected, thus increasing the linear density. A consequence of the reduced mark size is that the track pitch can be scaled down as well.

To achieve a high radial density a narrow track pitch is preferred. It is then very important to control the optical and thermal cross talk between tracks. Optical cross talk occurs when during reading the laser light is also reflected on adjacent tracks, causing distortions in the detected light intensity. It has been shown that by tuning the groove depth optical cross-track cross talk can be reduced to an acceptable level [33].

The occurrence of thermal cross-track cross talk during writing is a serious problem since thermal diffusion from the central track and light absorption in adjacent tracks can cause partial erasure of existing marks on the adjacent tracks. The temperature distribution has been shown to be dependent not only on the geometry of the grooved structure and the configuration of the recording stack, but also on the wavelength and polarization of the light. Furthermore, differences have been observed between land and groove recordings [36].

The choice of the recording scheme is another way of influencing a disks radial density. When land-groove recording is used the radial density can be increased, but the above mentioned cross talk phenomena then become an issue more strongly.

Recording speed is limited by the (re)crystallization time of the active material. During writing, pulse duration and intensity are to be taken such that the crystalline material melts within a period of time shorter than the crystallization time to prevent (complete) recrystallization. In addition, the individual amorphous dots should be sufficiently near to form a mark. During erasure, the spot should remain sufficiently long above an amorphous region to keep it at a temperature above the crystallization temperature for at least the crystallization time.

An increase of transfer rate can thus be realized by optimization of the composition of the active material. The reduction of the bit length by decreasing the spot size also enables faster recording speeds since smaller marks implicate shorter (re)crystallization times.

Chapter 3

The modeling of phase-change recording

The processes of data recording and erasing for rewritable optical disks can be described as a complex interaction of phenomena occurring in the fields of optics, thermodynamics and materials science. Due to the complexity, the direct modeling of these processes, i.e. as a whole, is impractical. Therefore the assumption is made that each process can be modeled separately. This subdivision will be explained in more detail in Section 3.1. In Sections 3.2-3.6 the subprocesses will be characterized and modeling aspects will be considered.

3.1 An overview of the modeling process

Before we discuss the modeling of recording and erasing of data for rewritable optical disks, let us first recall how these processes work. In optical recording of rewritable disks, binary data is written by applying short high power pulses with a laser beam that is focused on the PC-layer of the disk. As a consequence of the heating, the PC-material melts and the crystalline structure of the material is broken down. After the laser is switched off, the temperature rapidly drops from above the melting temperature to below the crystallization temperature (quenching). The stack design and material properties are taken such that the duration of the cooling down is shorter than the crystallization time of the PC material. Since no complete crystallization took place, an amorphous solid region is formed. A train of amorphous dots written shortly after another forms a mark.

The marks can be erased by applying the same focused laser beam, but now continuously set at a lower power level than during recording. The power

level is such that the temperature in the material rises above the material's crystallization temperature, but is kept below its melting temperature. Thus, during erasing, the PC-material does not melt. If the amorphous region is heated for a time period longer than the crystallization time, the amorphous material crystallizes completely, resulting in a fully crystalline solid material.

From the descriptions above it is clear that the modeling of the recording and erasing of data on rewritable optical disks, as a whole, is very complicated, since these processes are largely complex. This complexity is mainly due to the mutual dependencies of the various physical parameters involved. For example the focused laser beam causes a (locally) high rise of temperature in the disk as a result of which both the optical as well as the thermal parameters of the materials in the stack change. Another difficulty is that these processes take place on a sub-micron scale. Furthermore, a possible numerical model for these processes as a whole would inevitably lead to considerable demands on processor time, working memory and storage space.

Taking the complexity of the processes of recording and erasing into consideration, a plausible approach is to divide the general model into two parts. Both the recording as well as the erasing of data are induced by the energy contained in the incident light. Therefor, the first part will be the computation of the EM field distribution in the disk. From this EM field the light absorption in the medium can be derived. Recently, a so-called $2\frac{1}{2}$D optical model has been modified and further developed by Brusche [7] to be applied as part of a model of PC-recording. This optical model, that is used in the computation of the absorbed energy distribution in an optical rewritable disk, will be discussed briefly in the next section.

The second part is the modeling of the mark formation and mark erasure. Although both the formation and erasure of marks are temperature driven processes, they are essentially quite different, as will be explained later, and they will therefor be considered separately.

When modeling the mark formation, various degrees of accuracy can be sought for. An initial approach is to consider the formation of a mark as a simple threshold value determined growth process. Or to put it in other words, the size and shape of a mark are determined by whether the local rise of temperature during a laser pulse exceeds a given threshold value or not. The value used is in general taken to be (in relation to) the melting temperature of the PC-material. To obtain the temperature distribution in a 3D region of interest of the disk, the heat diffusion equation is (numerically) solved. It is assumed that the EM energy that is absorbed in the PC layer and the metal layer of the disk is totally converted into heat. This absorbed energy (per unit volume) then acts as the source term in the heat diffusion equation. The optical model as mentioned above can for instance be used

to compute the absorbed energy distribution. The computation of the temperature distribution as described above has been successfully implemented by Brusche [7]. In Section 3.3 this thermal model will be considered in more detail.

A more accurate and robust approach is to treat the mark formation process as a Stefan problem. A Stefan problem is a boundary value problem with an additional boundary condition that describes the movement of the interface in time. This extra condition is called the Stefan condition. For the mark formation problem the governing equation is the heat diffusion equation. The moving interface is the boundary between the fluid and solid phases of the PC material. The writing of a mark can thus be described as a two-phase Stefan problem. An interesting aspect of this formulation is that it incorporates latent heat, i.e. the energy required for a phase transformation, in a natural way. More details on the Stefan problem formulation will be given in Section 3.5.

A variety of numerical techniques exists for solving moving boundary problems. Two groups of methods can be distinguished: front-tracking methods and implicit methods. In the front-tracking methods the position of the interface is computed explicitly in each time step. Implicit methods use an alternative way of updating the interface position. A selection of numerical methods for solving moving boundary problems will be discussed in Chapter 4.

The erasure of a mark is characterized by (re)crystallization, i.e. the transition from an amorphous state to a crystalline state. As has been mentioned before, the crystallization process is also temperature driven. The temperature distribution required can for instance be obtained using the combined optical and thermal model by Brusche [7]. The crystallization itself can be described by a 3D nucleation and growth model. This model essentially envelopes a probability function, that predicts the jump of an atom from the amorphous state to a so-called critical nucleus of the crystalline state, and a function that describes the growth of the crystalline grain. Crystallization and the crystallization model are further discussed in Section 3.6.

We conclude this section by remarking that recrystallization also occurs at the mark boundary during writing. Taking this additional effect into account in the modeling of the writing process would pose new challenges, but is left out of consideration for the time being.

3.2 The computation of the absorbed energy distribution

Because the structure sizes of the medium are of the order of the wavelength of the laser spot, optical properties, such as the polarization of the light, cannot be neglected. As has been remarked in Section 2.2, a scalar model for the scattering of the light that is incident on the disk, can then not be used. A rigorous vector diffraction model based on Maxwell's equations is thus required.

Many vector diffraction models have been considered to derive the EM field distribution in grooved multi-layered stacks. These methods have been developed in the context of the optical readout of prerecorded DVD's. We refer to [28, 29, 31, 35, 36, 45] for some several examples.

Although the referenced models have lead to some interesting results, we prefer a model published by Brok and Urbach [6] and later extended by Brusche [7]. The model considered is based on the finite element method (FEM). Besides the fact that a lot is known about its mathematical properties, the FEM has certain advantages over other methods. The main advantage is that all kinds of geometries, such as bumped layers, can be simulated. The shape of the interfaces is not restricted and kinks are permitted. Furthermore, the presence of metals with negative real electric permittivity does not cause any problem.

Similar to Yeh et al. [45], the diffraction model by Brok and Urbach [6] for a 3D spot that is incident on a 2D periodic multi-layered recording stack, is based on a plane wave expansion of the spot. But the sampling is done such that the plane waves can be divided into sets that, for the given period of the grating, consist of waves which are orders of each other. This reduces the number of scattering problems that have to be solved considerably. The superposition of the plane waves in each set yields a quasi-periodic incident field whose interaction with the periodic grating can be computed by solving a single boundary value problem (BVP). This BVP is derived on a 2D computational box which is one period wide and is called a unit cell. Instead of approximative absorbing boundary conditions, exact radiation conditions for the scattered near field are used. The solution of the BVP is computed using FEM. The total EM field is obtained by coherently adding all scattered fields relating to all quasi-periodic incident fields.

In Brusche [7] the above described scattering model has been successfully extended to a 3D region of interest, i.e. to a region of the disk in which the amount of light energy that is absorbed has to be known for further temperature calculations. For further details, the reader is referred to the

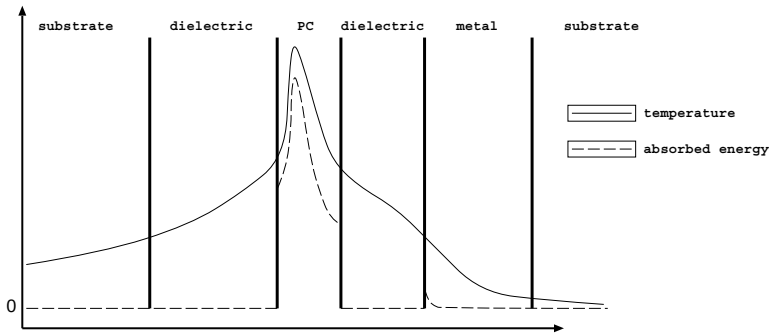

Figure 3.1: Sketch of the absorbed energy and temperature profile across the interfaces of a BD disk.

article.

When the total EM field is obtained, the amount of light absorption in the disk can be computed. It is assumed that in those layers of the recording stack that are absorbing the EM energy is entirely converted into heat. The rate Q at which heat is generated per unit volume, due to the absorption of light, is given by [21]:

$$Q(\mathbf{r}) = \frac{1}{2}\omega\epsilon_0 \mathrm{Im}\left[\epsilon(\mathbf{r})\right] |\mathbf{E}^{tot}(\mathbf{r})|^2, \tag{3.1}$$

where $\mathrm{Im}\left[\epsilon(\mathbf{r})\right]$ denotes the imaginary part of the electric permittivity at position $\mathbf{r}$.

Figure 3.1 shows a sketch of a typical absorbed energy profile across the interfaces of a BD stack. Note that the absorbed energy is a discontinuous quantity and in the non-absorbing layers of the disk it is of course equal to zero. Furthermore, in general almost all of the light energy is absorbed in the PC layer and the maximum amount of energy is absorbed near the interface between the PC layer and the first (and thickest) dielectric layer.

3.3 Direct computation of the temperature distribution

When one is interested in modeling the writing of marks, it is often useful to obtain a preliminary estimate of the mark shape and size. Such an estimate can be acquired from a simple model, such as will be explained in the next section, for which only the temperature distribution has to be known. Furthermore, knowledge of the distribution of the temperature in a disk is

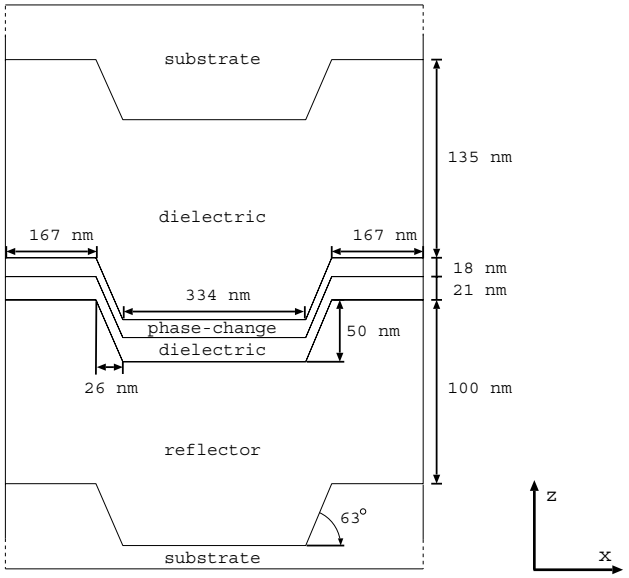

Figure 3.2: The geometry of a grooved BD stack. The groove depth and inclination angle have been exaggerated to make the differences between TE- and TM-polarized spots more distinct.

required to model the erasing of written marks. Next, we will discuss a simple 3D thermal model for acquiring the temperature distribution in a region of interest in a rewritable disk.

Let (x, y, z) be a Cartesian coordinate system that is parallel to the coordinate system of the optical model from Section 3.2. The chosen coordinate system moves with the disk at a speed v in the positive x-direction. The rise of temperature above ambient, $T(\mathbf{r})$, due to the heating of the disk by the spot between $t = 0$ and $t = t_e$, is computed by solving the (3D) heat diffusion equation:

$$\rho c \frac{\partial T}{\partial t} - \nabla \cdot [\kappa \nabla T] = Q(x, y - vt, z), \tag{3.2}$$

where κ is the heat conductivity, ρc is the specific heat and $Q(x, y, z)$ is given by (3.1). The heating does not necessarily have to be continuous at all times. A pulse strategy can also be applied.

The material properties are taken to be constant in the different layers of the PC-disk and are assumed to be independent of the temperature in the temperature range of interest. The computational domain is taken to be large enough such that putting $\partial T/\partial n = 0$ on the outer boundary $\delta\Omega$ is a realistic boundary condition.

The thermal model described above is used by Brusche [7] in combination with the optical model described in Section 3.2. This optical model has the limitation that changes in the optical properties of the medium, and thus in the absorbed energy distribution, cannot be taken into account in the 3D thermal model, because these changes are three-dimensional. But the effect of these changes on the light distribution in the stack, and in particular on the absorbed energy, are in general small.

In similar work, Peng and Mansuripur [36] successfully combined an optical and a thermal model to study thermal cross-track cross talk effects.

A sketch of a typical temperature profile across the interfaces of a rewritable disk is shown in Figure 3.1. In contrary to the absorbed energy, the temperature is continuous across the interfaces. A peak in the temperature is observed where the absorbed energy reaches its maximum value.

3.4 A simple mark formation model

As is often the case when modeling complex processes, a simple model in which various aspects of the process are left out of consideration, can lead to insight in the process. In the case of mark formation modeling, much can be learned about for instance the size and shape of a mark from an estimation. Such an estimate does not necessarily need to take into account the effects of the latent heat or recrystallization at the mark boundary.

The simple model discussed in this section could be called a threshold value model and it requires the temperature distribution in the disk to be known. The idea of the model is to assign all regions in the PC layer where the temperature has exceeded the melting temperature of the PC material to be amorphous. All others regions are taken to be crystalline. Hence, the possible existence of a 'mushy zone', i.e. a region in which the material is neither fully amorphous nor fully crystalline, is not considered.

As an illustration we consider the temperature distribution in a grooved BD stack as shown in Figure 3.2. The incident spot is taken to be Gaussian and predominantly TM-polarized. Figure 3.3 shows the temperature distribution after heating for 100 ns in a cross-section of the disk perpendicular to the grooves and parallel to the optical axis as found by Brusche [7]. In the figure an outline is shown of the estimated mark boundary in case the melting temperature of the PC material is approximately 650 $^{\circ}C$. Note that in this specific example small amorphous regions have formed on the adjacent lands. Based on this data it can be concluded that, when a land-groove recording strategy is used, cross-track interference effects can be expected.

Obviously, an estimate as obtained using the above model can be expected

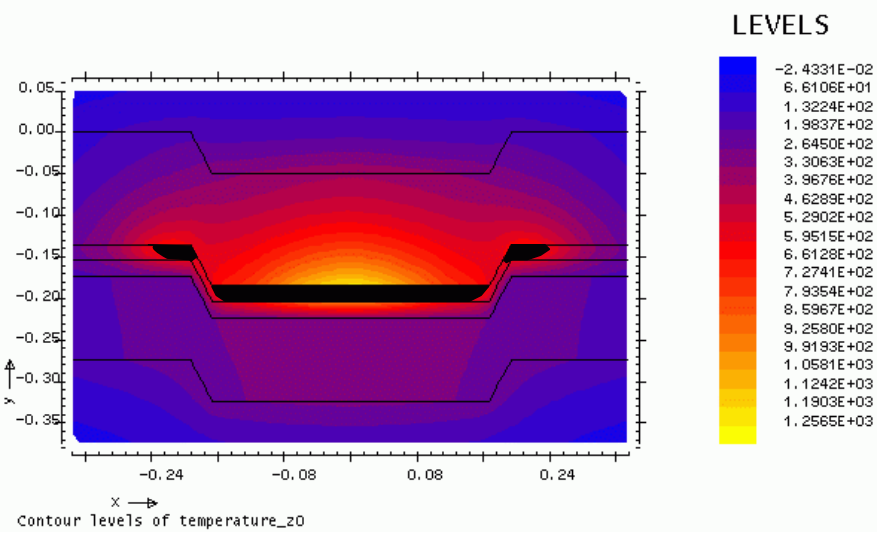

Figure 3.3: An estimate of a mark for a grooved BD stack based on a simple threshold value model.

to be quite inaccurate. Therefor, it is interesting to get an idea of how large an influence the exclusion of latent heat in the model has on determining the mark shape. To this end we compare the numerical values of the specific heat of the PC material, see Table 3.1, and the latent heat of the solid-to-liquid transition $L = 418.9\ J/cm^3$ as given in Ref. [8]. Since the specific heat $C \approx 1 J/cm^3/K$, this means that the melting of $1cm^3$ is approximately equal to heating up that same volume by $400K$. This implicates that latent heat might play a significant role in the mark formation process. Thus, a sizeable difference between the mark boundary as obtained with the threshold value model (i.e. without latent heat) and as acquired from solving a moving boundary problem (i.e. including latent heat), is to be expected.

Table 3.1: Numerical values for the specific heat C and heat conductivity κ.

	$C\ [J/cm^3/K]$	$\kappa\ [W/cm/K]$
substrate	1.7	0.0022
PC (amorphous)	1.285	0.0017
PC (crystalline)	1.285	0.005
PC (liquid)	1.285	0.005
dielectric	2.005	0.006
metallic mirror	2.45	0.25

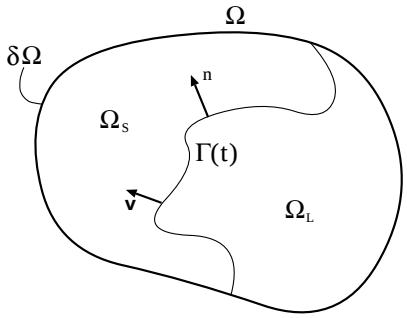

Figure 3.4: The domain Ω with the moving boundary $\Gamma(t)$.

3.5 A two-phase Stefan problem formulation

During the writing of a mark, the heating by the laser spot causes part of the initially solid crystalline PC material to melt. When the time needed for the temperature to drop below the crystallization temperature is much shorter than the crystallization time, most atoms in the liquid PC material will not recrystallize during solidification and a solid amorphous region, the mark, is formed.

In the following we will assume that during the solidification no recrystallization occurs. Consequently, the region that is considered to be amorphous will be the same region as that which is liquefied during heating. Likewise, the crystalline region is taken to correspond to the part of the material that stayed solid.

A second assumption is the non-existence of a so-called 'mushy zone' in which the PC material is neither fully liquid nor solid. Thus, the interface between the liquid and solid phase will be sharp. The simulation ends at time t_e.

Let Ω be the domain in 3D Cartesian space occupied by the PC material as depicted in Figure 3.4. As of a time t_m, $t_0 \leq t_m \leq t_e$, Ω is composed of two disjunct sub-domains $\Omega_s(t)$ and $\Omega_l(t)$, occupied by the solid and liquid phases of the PC material, respectively. These sub-domains are separated by a unknown surface $\Gamma(t)$ to be determined. The fixed outer boundary is denoted as $\delta\Omega$.

In each of the sub-domains the temperature rise above ambient $T(\boldsymbol{x}, t)$

satisfies the heat diffusion equation (3.2):

$$\rho_s c_s \frac{\partial T(\boldsymbol{x},t)}{\partial t} = \nabla \cdot (\kappa_s \nabla T(\boldsymbol{x},t)) + Q(\boldsymbol{x},t), \quad \forall \boldsymbol{x} \in \Omega_s, \quad t \in [t_0, t_e], \quad (3.3)$$

$$\rho_l c_l \frac{\partial T(\boldsymbol{x},t)}{\partial t} = \nabla \cdot (\kappa_l \nabla T(\boldsymbol{x},t)) + Q(\boldsymbol{x},t), \quad \forall \boldsymbol{x} \in \Omega_l, \quad t \in [t_m, t_e], \quad (3.4)$$

where we have omitted the speed v at which the spot moves over the disk. The coefficients $\rho_s, \rho_l, c_s, c_l, \kappa_s, \kappa_l$ are assumed constant, but may be different in each phase.

On the unknown moving boundary $\Gamma(t)$ two conditions have to be satisfied. First, the temperature equals the known melting temperature:

$$T(\Gamma(t), t) = T_m \quad (3.5)$$

and second the temperature has to satisfy the Stefan condition:

$$+\rho L v_n = \left[\kappa \frac{\partial T}{\partial n}\right] \quad (3.6)$$

where L is the latent heat, $\boldsymbol{n}$ is the (unit) normal vector on Γ pointing from $\Omega_l(t)$ to $\Omega_s(t)$, and v_n the normal velocity of the moving interface. By $[\phi]$ we denote the jump in ϕ defined as:

$$[\phi] = \lim_{\substack{\boldsymbol{x} \longrightarrow \Gamma(t) \\ \boldsymbol{x} \in \Omega_s(t)}} \phi(\boldsymbol{x},t) - \lim_{\substack{\boldsymbol{x} \longrightarrow \Gamma(t) \\ \boldsymbol{x} \in \Omega_l(t)}} \phi(\boldsymbol{x},t) \quad (3.7)$$

3.6 Crystallization

The processes of amorphization of molten regions during quenching and the crystallization of the amorphous state during erasing are very complicated. In order to model these processes, knowledge of the crystallization kinetics is of great importance.

Many of the existing descriptions of crystallization kinetics come from thermodynamics. They are mainly based upon two theories: Johnson-Mehl-Avrami-Kolmogorov (JMAK) theory and classical nucleation theory. In both theories it is assumed that crystallization occurs either by the nucleation of critical size particles and their subsequent growth within the untransformed region, or by the growth of crystallites at the boundary between the untransformed region and the surrounding crystalline matrix. With JMAK theory the volume fraction of crystallized material can be computed in terms of nucleation and growth rates. The classical nucleation theory allows for the

calculation of the nucleation and growth rates, and the distribution of the crystallite size.

According to Senkader et al. [38] both these approaches have inevitable limitations, mostly since in optical recording nucleation and growth occur within very short time scales. The authors remark that the nucleation in a real system not only involves clusters of critical size. The progress of the nucleation also depends on the interaction of the critical size nuclei with subcritical and supercritical sized clusters of molecules. Therefore, Senkader et al. propose a model to compute the distribution of cluster sizes. For another example of a dynamic theory, based on cluster concentrations, the reader is referred to [43].

Despite the more realistic modeling that the dynamic models provide for and the limitations of models based on either JMAK theory or the standard theory of kinetics, we will in the following only consider the classical crystallization model. A motivation for this choice is that the classical model gives an explicit formula for the growth velocity.

Next, we will first give an outline of the general idea of the nucleation and growth model by considering a very simplified, though illustrative, two dimensional example, based on the implementation by Peng et al. [8]. After the example we will subsequently discuss into detail the Gibbs free energy, nucleation and growth. In the sections on nucleation and growth we will mainly focus on the more general crystallization model as presented in [8]. A slightly simplified model assuming spherical nucleus growth [20, 40], will also be considered.

3.6.1 A simplified example

The recrystallization of an amorphous region of a section of PC material of unit thickness can for instance be modeled as follows. First the section of interest is discretized into $n \times n$ unit control volumes. Each control volume (or cell) can either be in the amorphous solid phase or the crystalline solid phase.

Each step, for every amorphous control volume there is a statistical probability that atoms will cluster and form a stable crystalline nucleus. This probability depends on temperature (averaged over the control volume) and the status of the adjacent cells, see Figure 3.5. If none of the four closest neighbors is crystalline, there is a probability $P_n(T)$ for a stable nucleus to be formed and the amorphous cell to become crystalline. Otherwise, when the amorphous cell has at least one crystalline neighbor, it has probability $P_g(T)$ to become crystalline through growth of the crystalline surroundings.

In case P_g is relatively large compared to P_n, the crystallization is called

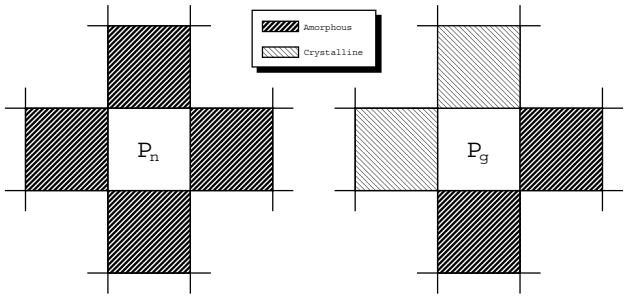

Figure 3.5: In the example of the simplified recrystallization model in the text, the probability that a cell transforms from the crystalline to the amorphous state depends on the state of its nearest neighbors.

growth dominated. When P_n is relatively larger than P_g, the crystallization is called nucleation dominated.

Figures 3.6 and 3.7 show results of a simulation of the recrystallization of a mark, consisting of three overlapping amorphous dots, in case of growth dominated crystallization and nucleation dominated crystallization, respectively. For simplicity, in these simulations P_n is assumed to be independent of temperature and the probability P_g has been replaced by a prescribed rate of growth: in the growth dominated case every step an amorphous cell with at least one crystalline neighbor becomes crystalline; for nucleation dominated crystallization this happens every fifth step. We stress that the probabilities and growth rate in this example have been chosen such that the difference between nucleation dominated and growth dominated crystallization is evident, and are not related to any realistic situation.

Even though the example uses a very simplified model, it clearly shows the distinct difference between nucleation dominated and growth dominated recrystallization. Before we come to describe the crystallization process, it is important to first understand the driving force behind this process, the so-called Gibbs free energy. The following section contains fragments taken from [24].

3.6.2 Gibbs free energy

Some reactions are spontaneous because they give off energy in the form of heat ($L < 0$). Others are spontaneous because they lead to an increase in the disorder of the system ($\Delta S > 0$). Calculations of the change of enthalpy L and the change of entropy ΔS can be used to probe the driving force behind a particular reaction. In order to understand what happens when one of the potential driving forces behind a chemical reaction is favorable and the other

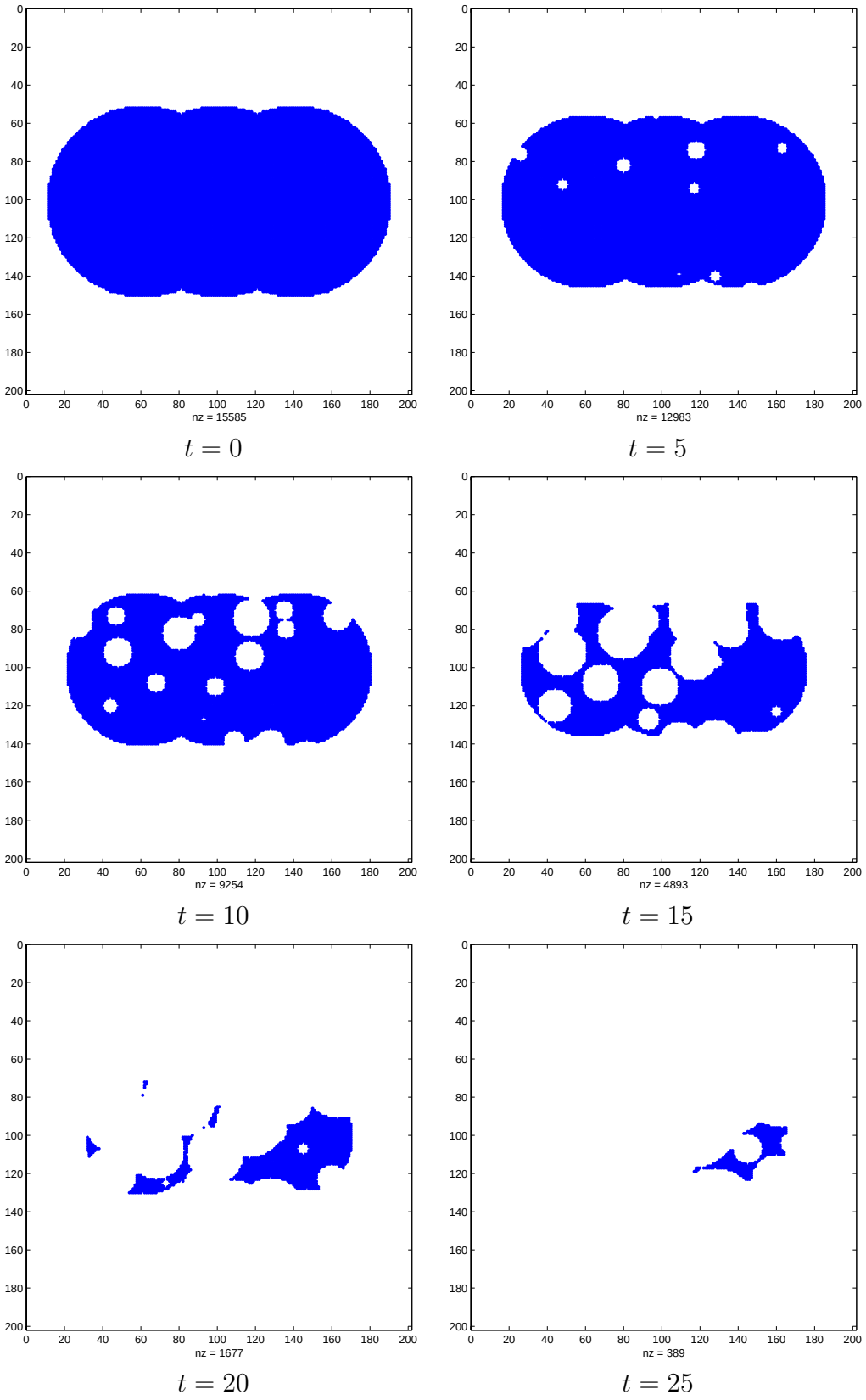

Figure 3.6: An example of growth dominated recrystallization. The amorphous/crystalline interface expands at one control volume per step. The nucleation probability P_n for an amorphous control volume is < 0.0001. The complete mark is erased at $t = 31$. nz is the number of amorphous control volumes.

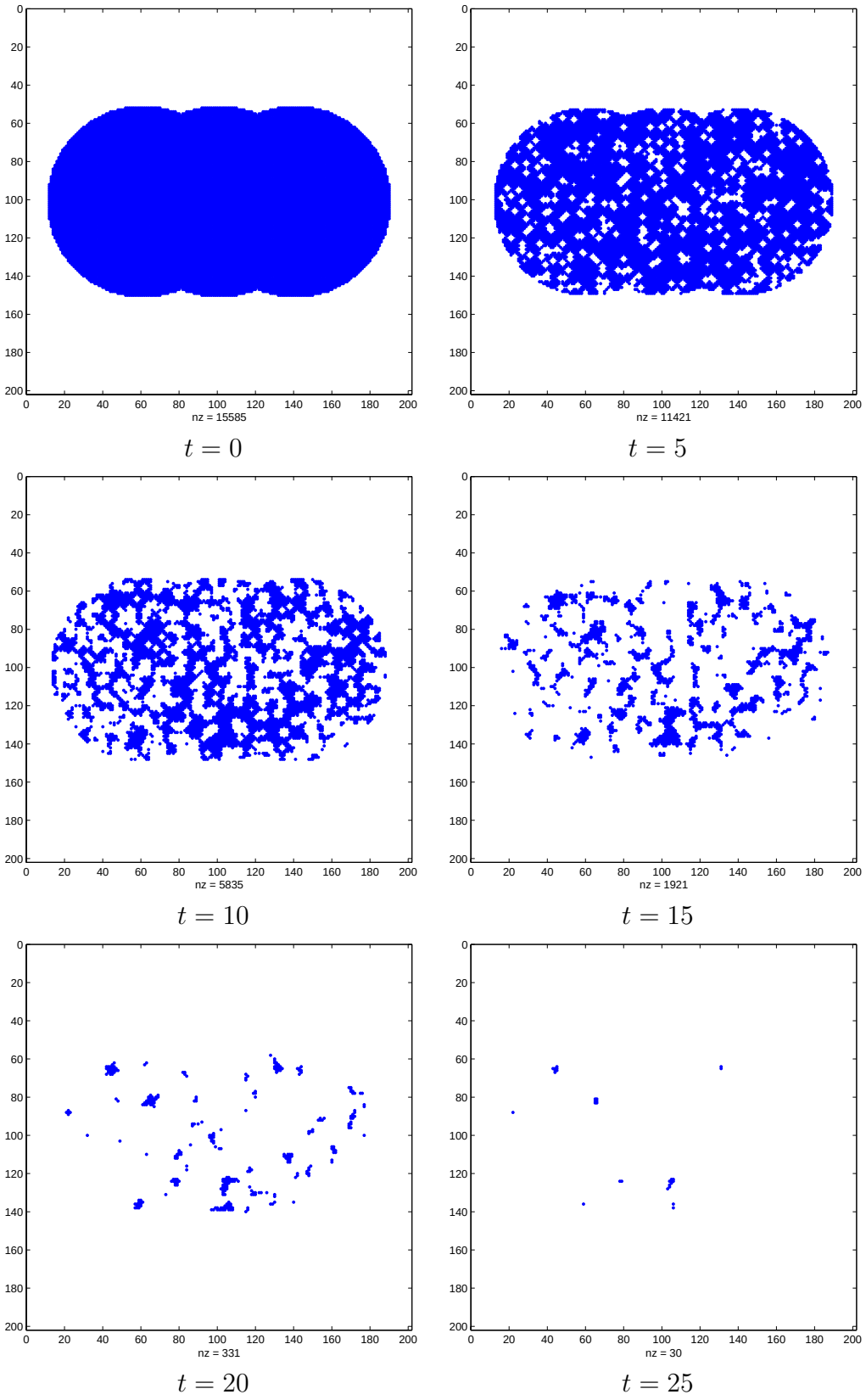

Figure 3.7: An example of nucleation dominant recrystallization. The amorphous/crystalline interface expands at one fifth of a control volume per step. The nucleation probability P_n for an amorphous control volume is < 0.005. The complete mark is erased at $t = 30$. nz is the number of amorphous control volumes.

is not, one can consider the balance between these forces, known as the Gibbs free energy. The Gibbs free energy G of a system at any moment in time is defined as the enthalpy of the system minus the product of the temperature times the entropy of the system: $G = H - TS$.

The Gibbs free energy of the system is a state function because it is defined in terms of thermodynamic properties that are state functions. The change in the Gibbs free energy of the system that occurs during a reaction is therefore equal to the change in the enthalpy of the system minus the change in the product of the absolute temperature T times the entropy of the system.

$$\Delta G = L - \Delta(TS) \tag{3.8}$$

If the reaction is run at constant temperature, this equation can be written as follows.

$$\Delta G = L - T\Delta S \tag{3.9}$$

As we have seen, the enthalpy and entropy terms have different sign conventions. The entropy term is therefore subtracted from the enthalpy term when calculating ΔG for a reaction.

favorable	unfavorable
$L < 0$	$L > 0$
$\Delta S > 0$	$\Delta S < 0$

Because of the way the free energy of the system is defined, ΔG is negative for any reaction for which L is negative and ΔS is positive.

Reactions are classified as either exothermic ($L < 0$) or endothermic ($L > 0$) on the basis of whether they give off or absorb heat. Reactions can also be classified as exergonic ($\Delta G < 0$) or endergonic ($\Delta G > 0$) on the basis of whether the free energy of the system decreases or increases during the reaction.

The balance between the contributions from the enthalpy and entropy terms to the free energy of a reaction depends on the temperature at which the reaction is run. The equation used to define Gibbs free energy (3.9) suggests that the entropy term will become more important as the temperature increases. Since the entropy term is unfavorable, the reaction should become less favorable as the temperature increases.

3.6.3 Nucleation

In the amorphous phase, there is a statistical probability that atoms will momentarily form a crystalline cluster. These so-called embryos are potential

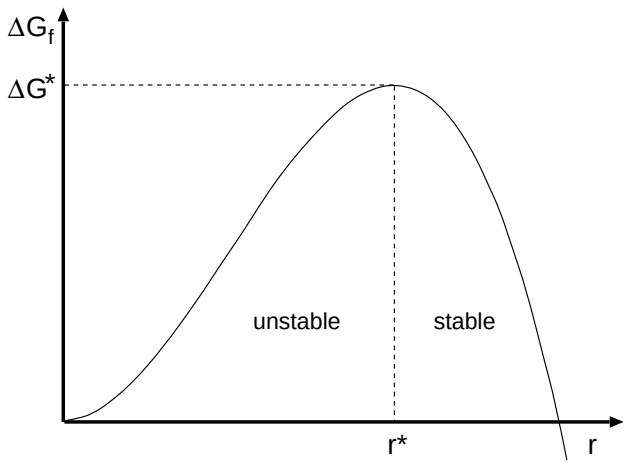

Figure 3.8: The heat of formation ΔG_f as a function of the radius r (for spherical nuclei). For a potential cluster to become stable, i.e. to form a crystalline nucleus, the net difference in Gibbs free energy between an unstable and a stable cluster must exceed the energy barrier ΔG^*.

nuclei for the crystallization process. Clusters that exceed some critical size can reduce the system free energy only through further growth and hence stable nuclei are capable of sustained existence. Sub-critical clusters decrease the system free energy via shrinking in size and thus will tend to dissolve back in to the parent phase [37]. The Gibbs free energy per volume of the crystalline state is lower than that of the amorphous phase. The change of Gibbs free energy ΔG_n, or excess Gibbs free energy, corresponding to the crystalline-to-amorphous transition is given by (3.9):

$$\Delta G_n = L - T\Delta S \tag{3.10}$$

In order for an embryo to transform into a stable nucleus, the so-called heat of formation ΔG_f, which is the net Gibbs free energy between a stable nucleus and an embryo, has to exceed the activation energy ΔG^*, or energy barrier.

For spherical nuclei of radius r, the heat of formation is given by [40]:

$$\Delta G_f = f(\theta)\left(A\gamma - V\Delta G_n\right) = f(\theta)\left(4\pi r^2\gamma - \frac{4\pi r^3}{3}\Delta G_n\right) \tag{3.11}$$

where V is the volume and A the surface area of the nucleus, γ is the interface energy and $f(\theta)$ is a function of contact angle θ. For homogeneous nucleation, $f(\theta) = 1$ and the energy barrier ΔG^* is equal to the maximum of $\Delta G_f(r)$. At the critical radius $r^* = 2\gamma/\Delta G_n$ this maximum is reached:

$$\Delta G^* = \frac{16\pi}{3}\frac{\gamma^3}{\Delta G_n^2} f(\theta) \tag{3.12}$$

In case of inhomogeneous nucleation, i.e. in the presence of impurities, which lower the interface energy, the critical free energy is reduced. Therefore, $f(\theta) < 1$ for inhomogeneous nucleation.

Note that for large radii r the volume related term in equation (3.11) is dominant, while for small clusters the surface term dominates. This is of special importance when considering the effect of the thickness of the PC layer on the crystallization behavior.

When arbitrarily shaped nuclei are considered the energy barrier is given by:

$$\Delta G^* = \tilde{A}\frac{\gamma^3}{\Delta G_n^2} f(\theta) \tag{3.13}$$

where $\tilde{A}$ is related to the volume and surface area of the nucleus and is temperature dependent. However, as has been remarked in [8], we will assume $\tilde{A}$ to be temperature independent, in which case its value may be determined from the peak temperature T_N at which the rate of nucleation is at maximum.

The temperature dependence of the excess Gibbs free energy (3.10) may be approximated by

$$\Delta G_n = \begin{cases} L_2 \left[1 - \frac{T}{T_g}\left(1 - \frac{L_1}{L_2}\frac{T_m - T_g}{T_m}\right)\right] & T \leqslant T_g \\ L_1 \frac{T_m - T}{T_m} & T > T_g \end{cases}, \tag{3.14}$$

where L_1 and L_2 are the latent heat of the solid-to-liquid transition and the exothermic heat of the amorphous-to-crystalline transformation, respectively, T_g is the glass transition temperature and T_m is the melting temperature.

The (time-independent) rate of nucleation I can be expressed as:

$$I = \alpha \exp\left(-\beta \left[E_{a_1} + \Delta G^*\right]\right). \tag{3.15}$$

Here, α is a frequency factor related to the atomic jumping frequency; $\beta = 1/k_B T$, where k_B is the Boltzmann constant; E_{a_1} is the activation energy associated with the jump of an atom from the amorphous phase to the critical nucleus of the crystalline phase. For spherical nuclei, ΔG^* is given by equation (3.12). Otherwise, equation (3.13) applies.

The probability for an untransformed grid volume ΔV to become a crystalline nucleus during a time interval Δt is then given by

$$P_n = I \Delta t \Delta V. \tag{3.16}$$

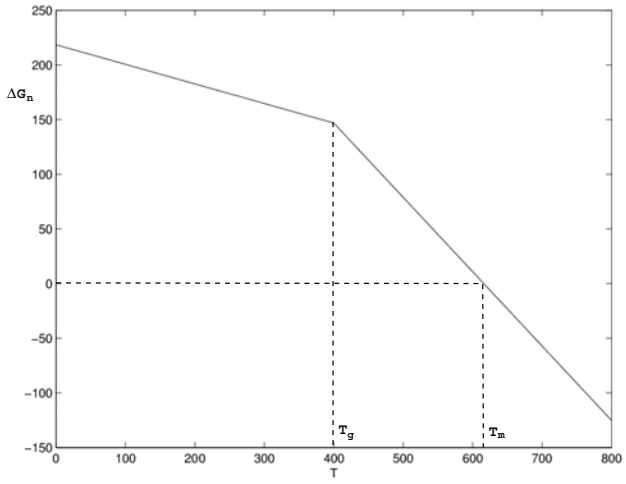

Figure 3.9: Approximation of the temperature dependence of the excess Gibbs free energy ΔG_n as in (3.14). The numerical values as in Table 3.2 have been used.

3.6.4 Growth

Besides through nucleation, an amorphous region may become crystalline by growing from an adjacent nucleus or from the boundary of the surrounding crystalline regions. The growth velocity V_g of a crystallite is written as:

$$V_g = g a_0 \alpha \exp(-\beta E_{a_2})[1 - \exp(-\beta \Delta G_n)], \tag{3.17}$$

where g is a factor related to the growth mode; a_0 is the atomic jump distance; and E_{a_2} is the activation energy associated with the diffusion of atoms. In order to simulate lateral growth, [8] assume g to be proportional to $\exp[-0.8/(1 - T/T_m)]$.

The growth probability for an untransformed grid volume ΔV is then given by

$$P_g = V_g \Delta t \Delta V. \tag{3.18}$$

In case spherical grain growth is assumed the nucleus radius can be directly calculated from the growth velocity as

$$r(t) = \sum_{t>\tau} V_g \Delta t / g, \tag{3.19}$$

where τ is the time at which this grain nucleated.

The numerical values of some of the quantities mentioned above are listed in Table 3.2.

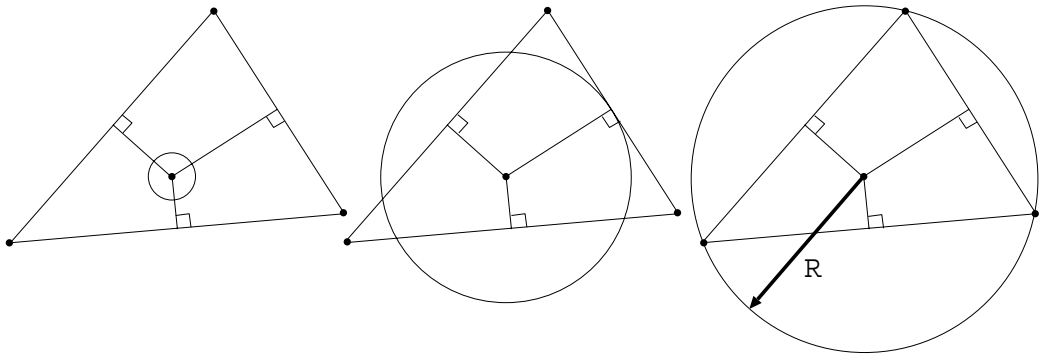

Figure 3.10: A spherical crystallite growing in the circumcenter of a mesh triangle.

For the crystallization model as presented above, it is likely that a much finer grid is used than that of the melting and solidification model. As long as the crystallites are smaller than a grid cell of the coarser mesh, growth can be modeled using the above described growth model. As soon as the crystallites have grown beyond the grid size of the coarser mesh, the consecutive growth can be modeled using a moving boundary method.

Remark: In case a FEM is used for computing the temperature distribution, a possible method of including a recrystallization model on the same mesh could be the following. Assume that in 2D a triangulation of the region of interest has been performed. As control volumes (areas) for the recrystallization model we then choose the triangles of the mesh. Each triangle which is fully amorphous then has a probability $\tilde{P}_n$ that a stable nucleus will form inside the triangle. When a nucleus has formed, we assume that it is located in the circumcenter of the triangle, see Figure 3.10. The nucleus is then assumed to grow at a speed $\tilde{V}_g$. If the radius of the nucleus has become larger than the circumradius, the triangle is considered to be fully crystalline. Besides, since the nucleus has grown beyond the grid size of the mesh, it's consecutive growth can be modeled using a moving boundary method.

Table 3.2: Numerical values of the kinetics parameters of a $Ge_2Sb_2Te_5$ alloy as given in Reference [8].

symbol	value	unit
E_{a_1}	2.19	eV
E_{a_2}	2.23	eV
T_m	616	$°C$
T_N	405	$°C$
T_g	400	$°C$
L_1	418.9	J/cm^3
L_2	218.5	J/cm^3
α	4×10^{25}	s^{-1}

Chapter 4

A survey of numerical methods

In this chapter we will present a survey of numerical methods for solving melting and solidification problems. In particular we are interested in finding a suitable numerical method to obtain the solution of the three-dimensional two-phase Stefan problem as introduced in Section 3.5. Most of the methods mentioned in this chapter have been developed in the more general context of phase-change problems, and aim at describing the evolution of temperature in time and either implicitly or explicitly keep track of one (or multiple) interfaces between phases.

We will first consider an analytical method, known as Neumann's method. This is of particular interest since problems for which an analytical solution exists, often appear in the literature in order to validate a numerical method.

Without attempting to be complete we will then briefly discuss a selection of numerical methods, other than the level set or enthalpy based ones, in Section 4.2. The main reason for including these methods in this survey is that, although we initially aim at either applying a level set or enthalpy based technique, knowledge of their benefits and drawbacks can prove useful once we have chosen a suitable method for solving our Stefan problem.

Finally, we will focus on numerical methods that use either an enthalpy or level set approach. The basic ideas behind methods based on an enthalpy formulation and level set based methods, will be successively presented in Sections 4.3 - 4.4. Both finite difference and (extended) finite element approaches will considered. In the conclusive section the benefits and drawbacks of the discussed methods will be compared.

4.1 Analytical methods

Analytical solutions exist for only a select number of phase-change problems. Stefan [39] was the first to solve the simplest phase-change problem possible: the one-dimensional one-phase problem in a semi-infinite region. By 'one-phase' we mean that, for a melting problem, only the liquid phase is 'active' while the other phase stays at the melting temperature, and is 'in-active'. Thus, to put it other words, only for the 'active' phase the heat diffusion equation has to be solved.

In the context of (1D) Stefan problems, a dimensionless number St given by

$$St = \frac{C_l(T_l - T_m)}{L}. \tag{4.1}$$

often appears in the literature. This number, generally known as the Stefan number, governs the rate of melting or solidification in a semi-infinite region. In (4.1), C_l is the heat capacity of the liquid, L is the latent heat of fusion and T_l and T_m are the temperatures of the surroundings and the melting point, respectively.

In the following we will consider Neumann's method for a two-phase Stefan problem. The problem description and most of the notation used are adopted from [25].

4.1.1 Neumann's method

In two-phase Stefan problems, both the liquid phase as well as the solid phase are 'active'. If melting of a semi-infinite slab ($0 < x < \infty$) is considered, initially solid at a uniform temperature $T_s < T_m$, and a constant temperature is imposed on the face $x = 0$, with assumptions of constant thermo-physical properties, the problem can be mathematically expressed as follows:

Heat conduction in the liquid region:

$$\frac{\partial T_l}{\partial t} = \alpha_l \frac{\partial^2 T_l}{\partial x^2} \qquad \text{for } 0 < x < \Gamma(t), t > 0 \tag{4.2}$$

Heat conduction in the solid region:

$$\frac{\partial T_s}{\partial t} = \alpha_s \frac{\partial^2 T_s}{\partial x^2} \qquad \text{for } \Gamma(t) < x, t > 0. \tag{4.3}$$

Interface temperature:

$$T(\Gamma(t), t) = T_m \quad \text{for } t > 0. \tag{4.4}$$

Stefan condition:

$$\kappa_s \frac{\partial T_s}{\partial x} - \kappa_l \frac{\partial T_l}{\partial x} = L\rho \frac{d\Gamma}{dt} \qquad \text{for } x = \Gamma(t), t > 0. \tag{4.5}$$

Initial conditions:

$$T(x,0) = T_s < T_m \qquad \text{for } x > 0, \Gamma(0) = 0. \tag{4.6}$$

Boundary conditions:

$$T(0,t) = T_l > T_m \qquad \text{for } t > 0, \tag{4.7}$$

$$T(x,t) = T_s \qquad \text{for } x \to \infty, t > 0. \tag{4.8}$$

Here $\alpha_l = \kappa_l / C_l$ and $\alpha_s = \kappa_s / C_s$ denote the thermal diffusivity of the liquid and the solid phase, respectively.

The exact solution to such a problem was obtained by Neumann in terms of a similarity variable

$$\eta_p = \frac{x}{2\sqrt{\alpha_p t}} \tag{4.9}$$

where the subscript p can be either l for the liquid phase or s to indicate the solid phase. The final Neumann's solution can be written as:

Interface position:

$$\Gamma(t) = \frac{x\lambda}{\eta_l}. \tag{4.10}$$

Temperature in the liquid phase:

$$T(x,t) = T_l - (T_l - T_m)\frac{\operatorname{erf}(\eta_l)}{\operatorname{erf}\lambda}. \tag{4.11}$$

Temperature in the solid phase:

$$T(x,t) = T_s - (T_m - T_s)\frac{\operatorname{erfc}(\eta_s)}{\operatorname{erfc}(\lambda\sqrt{\alpha_l/\alpha_s})}. \tag{4.12}$$

The λ in equations (4.10)-(4.12) is the solution of the transcendental equation

$$\frac{St_l}{\exp(\lambda^2)\operatorname{erf}(\lambda)} - \frac{St_s\sqrt{\alpha_s}}{\sqrt{\alpha_l}\exp(\alpha_l\lambda^2/\alpha_s)\operatorname{erfc}(\lambda\sqrt{\alpha_l/\alpha_s})} = \lambda\sqrt{\pi}, \tag{4.13}$$

where

$$St_l = \frac{c_l(T_l - T_m)}{L} \qquad St_s = \frac{c_s(T_m - T_s)}{L}. \tag{4.14}$$

Neumann's solution as presented above exists only for moving boundary problems in the rectangular coordinate system. An exact solution for phase-change problems in the cylindrical coordinate as well as several approximative methods can be found in the literature, but we will not discuss them here.

4.2 A brief overview of various numerical methods

The excellent paper by Hu and Argyropoulos [25] gives an elaborate review of numerical methods for modeling solidification and melting problems (for up until 1996). Because of the contents of this paper we will in this section limit ourselves to briefly summarizing the paper's third section on numerical methods for solving the pure heat conduction equation with a phase-change involved, so that detailed descriptions of the methods will be omitted. Except for some additional references to more recent publications (later than 1996), further references have also been omitted, as they can be found in the paper by Hu et al. In particular we will put emphasis on the benefits and drawbacks of the discussed methods. Unless stated otherwise, in the following it is assumed that a 1D heat diffusion problem is considered, but remarks on the extensibility to higher dimension will be made. Enthalpy and level set methods will be discussed separately in later sections.

The first class of methods we will discuss are the fixed grid methods. In a fixed grid method, the heat diffusion equation is for instance approximated by finite difference replacements for the derivatives in order to compute the values of the temperatures $T_{i,n}$ at location $x_i = i\Delta x$ and time $t_n = n\Delta t$ on a fixed grid in the (x, t) plane. It is assumed that at any time t_n the moving boundary is located between two adjacent grid points.

Various approximations have been proposed for the Stefan conditions on the moving boundary and the partial differential equation at the adjacent grid points, such as Taylor expansion based interpolations or Lagrange interpolations. Several efforts have been made to apply these and related techniques in both two and three space dimensions.

Probably the most problematic aspect of the fixed grid methods is the loss of accuracy associated with singularities, which can arise when the moving boundary is too near a grid point. The mathematical manipulations to resolve this are considered to be very lengthy and complex indeed. According to Hu et al., the mayor advantage of the fixed grid methods is that these methods can efficiently handle problems with multiple phase-fronts without much difficulty. Altogether, the elaborateness of properly dealing with singularities, especially in higher dimension, makes that the fixed grid methods might not be favorable for solving our Stefan problem.

Variable grid methods provide a solution for most of the drawbacks of the fixed grid methods. The variable grids can be either interface-fitting or dynamic. In interface-fitting grid methods (or variable time step methods) a uniform spatial grid but a non-uniform time step are used. At each new

time step the step size is chosen such that the moving boundary is located on a grid point. In dynamic grid methods (or variable space grid methods) the number of spatial intervals are kept constant and the spatial intervals are adjusted in such a manner so that the moving boundary lies on a particular grid point.

In [23] this technique is employed for two-dimensional two- and three phase solidification problems. The method presented is capable of dealing with freezing fronts that may have high curvatures. Christopher [12] compares an interface-following scheme using either a first- or second-order discretization with an enthalpy model (see 4.3). From the results of the performed computations it is concluded that the interface following method must use the second-order model for the moving interface to maintain the accuracy for fast-moving interfaces. In contrary to the enthalpy method, the interface following method cannot be used to model very complex shapes, such as intersecting phase-change interfaces. The enthalpy method also appears to be the most accurate of the methods considered in the article.

Although the adaptive grid approaches deal with many of the drawbacks of the fixed grid methods, the variable grid methods still mostly suffer from their inherent complexity, in particular for higher dimensional cases.

4.3 Enthalpy methods

When compared to the previously described methods, the enthalpy methods we will discuss next can be considered to be the most versatile, convenient, adaptable and easily programmable numerical methods for phase-change problems in 1, 2 or 3 space dimensions [2], Chapter 4.2. But, there are still many problems for which even an enthalpy approach is not suitable. Such is the case for instance for problems involving super-cooling, where the instability of the interface must be studied. Finding a weak formulation is then often impossible, due to the special interface conditions that are imposed. Alternatively, such problems can be solved using a phase-field approach (for instance see [16], Chapter 11, and references therein).

Before we come to explain the basics behind the enthalpy based methods we will first recall the two-phase Stefan problem from Section 3.5. On a three-dimensional domain Ω with fixed outer boundary $\delta\Omega$ and moving boundary

$\Gamma(t)$, the two-phase Stefan problem is given by:

$$\begin{cases} \rho c \dfrac{\partial T(\boldsymbol{x},t)}{\partial t} = \nabla \cdot (\kappa \nabla T(\boldsymbol{x},t)) + Q(\boldsymbol{x},t) & \forall \boldsymbol{x} \in \Omega_{1,2}, t > 0 \quad (4.15a) \\ +\rho L v_n = \left[\kappa \dfrac{\partial T}{\partial n} \right] & \text{for } \boldsymbol{x} = \Gamma(t), t > 0 \quad (4.15b) \\ T(\boldsymbol{x},0) = \bar{T}_1(\boldsymbol{x}) & \forall \boldsymbol{x} \in \Omega_{1,2}, t > 0 \quad (4.15c) \end{cases}$$

where we have set $t_0 = 0$, together with one or more of the following boundary conditions on the complementary parts $\delta\Omega_i, i = 1,2,3$ of the fixed outer boundary $\delta\Omega = \bigcup_{i=1}^{3} \delta\Omega_i$:

1. A Dirichlet condition on $\delta\Omega_1$:

$$T = \bar{T}_2(\boldsymbol{x}). \tag{4.16}$$

2. A Neumann condition on $\delta\Omega_2$:

$$\kappa(T) \frac{\partial T}{\partial \boldsymbol{n}}(\boldsymbol{x}) = \bar{q}(\boldsymbol{x}), \tag{4.17}$$

   where $\mathbf{n}$ is the outward unit normal to the boundary surface, and $\bar{q}(\boldsymbol{x})$ a given normal heat flux.

3. A radiation-type boundary condition on $\delta\Omega_3$:

$$\kappa(T) \frac{\partial T}{\partial \boldsymbol{n}}(\boldsymbol{x}) = \bar{\alpha}(T), \tag{4.18}$$

   where $\bar{\alpha}(T)$ is a non-linear function of temperature.

4.3.1 General description

The most convenient starting point for deriving a numerical scheme for solving the Stefan problem above, is to consider the law of energy conservation in the form of a primitive integral heat balance over arbitrary volumes and time-intervals, as given by

$$\int_t^{t+\Delta t} \frac{\partial}{\partial t} \left(\int_V H dV \right) dt = \int_t^{t+\Delta t} \int_{\delta V} -\mathbf{q} \cdot \mathbf{n} dS dt + \int_t^{t+\Delta t} \int_V Q dV dt. \tag{4.19}$$

Here, H is the energy density (per unit volume), or enthalpy, and $-\mathbf{q}\cdot\mathbf{n}$ is the heat flux *into* the volume V across its boundary δV, $\mathbf{n}$ is the outgoing normal to δV and Q is an internal heat source. The heat conduction equation (4.15a) can be easily derived from (4.19), see for instance [2], Chapter 4.1.

The energy balance (4.19) is valid irrespectively of phase over the whole domain considered, and even for jumps in H or $\mathbf{q}$. Thus, it is more general than the localized differential form

$$H_t + \operatorname{div}\mathbf{q} = Q. \tag{4.20}$$

According to the Gauss' divergence theorem, the integral notation (4.19) and the differential form (4.20) are equivalent for smooth $H, \mathbf{q}$ and Q. In case of a phase-change problem, (4.20) can only be interpreted classically (point-wise) in each phase separately, but then in addition a Stefan interface condition (4.15b) is required, making front-tracking necessary.

Alternatively, (4.20) may be interpreted in a weak sense globally. The numerical solution to the discretized form of equation (4.20) via the enthalpy method, is found to approximate the weak solution (see for instance [2], Chapter 4.4). It is for this reason that from this point onwards, as is common in the literature, to consider (4.20).

In general, the enthalpy function H is defined as the integral of the heat capacity with respect to temperature. For problems in which no phase-change occurs, the enthalpy H is equal to the sensible heat, defined by:

$$H(T) = \int_{T_{ref}}^{T} \rho c(T) dT, \tag{4.21}$$

where $\rho c = C$ is the volumetric heat capacity which depends on temperature, and where T_{ref} is a reference temperature. For problems involving a phase-change the enthalpy is defined as the sum of the sensible and the latent heat. Since the type of material considered influences the form of the function $H(T)$, it is convenient to distinguish between two cases: the non-isothermal (or mushy) phase-change, and the isothermal phase-change.

In case of isothermal phase-change, the enthalpy function has a jump-discontinuity at the melting temperature T_m and its temperature dependence may be written as:

$$H(T) = \begin{cases} \int_{T_{ref}}^{T} \rho c_s(T) dT, & \text{for } T \leq T_m, \\ \int_{T_{ref}}^{T_m} \rho c_s(T) dT + \rho L + \int_{T_m}^{T} \rho c_l(T) dT, & \text{for } T > T_m. \end{cases} \tag{4.22}$$

The quantity ρL, where L is the latent heat, is the energy that is required for a phase transition from the solid to the liquid state. If for example we

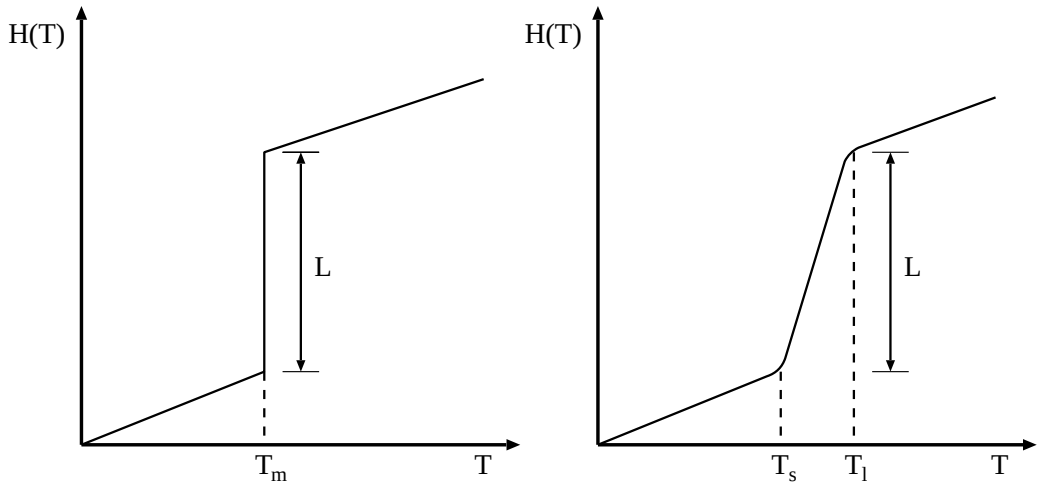

Figure 4.1: Sketches of the enthalpy versus temperature relations for isothermal phase-change (left) and mushy phase-change.

consider the case in which c_s, c_l are constants and $T_{ref} = T_m$ then (4.22) becomes

$$H = \begin{cases} \rho c_s (T - T_m), & T \leq T_m \\ \rho c_l (T - T_m) + \rho L, & T > T_m \end{cases} \tag{4.23}$$

That is, solving for T,

$$T = \begin{cases} T_m + \frac{H}{\rho c_s}, & \text{for } H \leq 0, \quad (solid) \\ T_m, & \text{for } 0 < H \leq \rho L, \quad (mushy) \\ T_m + \frac{H - \rho L}{\rho c_l}, & \text{for } H > \rho L \quad (liquid). \end{cases} \tag{4.24}$$

A more general form of phase-change, often appearing in industrial applications involving alloys, is that of mushy phase-change. In these problems melting takes place over a finite interval $[T_s, T_l]$. For non-isothermal cases the enthalpy function (4.21) takes the form:

$$H(T) = \begin{cases} \int_{T_{ref}}^{T} \rho c_s(T) dT, & \text{for } T \leq T_s, \\ \int_{T_{ref}}^{T_s} \rho c_s(T) dT + \int_{T_s}^{T} \rho \frac{\partial L}{\partial T} dT, & \text{for } T_s < T \leq T_l, \\ \int_{T_{ref}}^{T_s} \rho c_s(T) dT + \rho L + \int_{T_l}^{T} \rho c_l(T) dT, & \text{for } T > T_l. \end{cases} \tag{4.25}$$

In Figure 4.1 the enthalpy versus temperature relations in case of isothermal and mushy phase-change have been sketched.

The enthalpy formulation removes the necessity of carefully tracking the moving interface and consequently standard numerical techniques can be employed. Since in the enthalpy method the moving interface is not explicitly tracked, but the front position may be recovered from the values of the enthalpy a posteriori, the method may be characterized as a front-capturing scheme.

The procedure of the enthalpy method is roughly the following. For the sake of clarity, we assume that the parameters ρ, c and κ are constants for each phase and that an explicit time integration scheme is used. We partition the domain Ω into a finite number of cells V_i and apply energy conservation, as in equation (4.19), to each control volume to obtain a discrete heat balance. Given an initial state for which the specific heat, conductivity and temperature (and thus the phase) are known, this discrete form is used to update the enthalpy. The 'new' states of phase are then found by the enthalpy alone and the updated temperatures then follow from equation (4.24). The specific heat and conductivity for the new state are then easily determined.

In the next two sections we will successively discuss finite volume schemes and finite element approaches for solving the enthalpy equation. Since the 'standard' finite volume discretization methods discussed in the following can be extended to higher dimensions without much difficulty, we will restrict ourselves for clarity to one spatial dimension. For both finite volume and finite element techniques we will first consider the general theory. We conclude each section with a discussion of recently published articles on enthalpy methods.

4.3.2 Finite volume approaches

Consider a space-time grid as shown in Figure 4.2. The conductive flux across a face located at $x_{i-\frac{1}{2}}$ or $x_{i+\frac{1}{2}}$ of a control volume V_i is given by

$$q = -\kappa \frac{\partial T}{\partial x}. \tag{4.26}$$

To obtain a numerical scheme we introduce the discrete approximations

$$H_i^n \approx H(x_i, t_n), \quad q_{i\pm\frac{1}{2}}^{n+\theta} \approx q(x_{i\pm\frac{1}{2}}, t_n + \theta \Delta t_n), \quad 0 \leq \theta \leq 1, \tag{4.27}$$

in which we use the superscript notation for the flux defined as

$$q^{n+\theta} := (1-\theta) q^n + \theta q^{n+1} \tag{4.28}$$

so that we can write (4.20) as

$$\frac{H_i^{n+1} - H_i^n}{\Delta t_n} = \frac{q_{i-\frac{1}{2}}^{n+\theta} - q_{i+\frac{1}{2}}^{n+\theta}}{\Delta x_i} + Q_i^{n+\theta}, \quad i = 1, \ldots, M, \quad n = 0, 1, \ldots \tag{4.29}$$

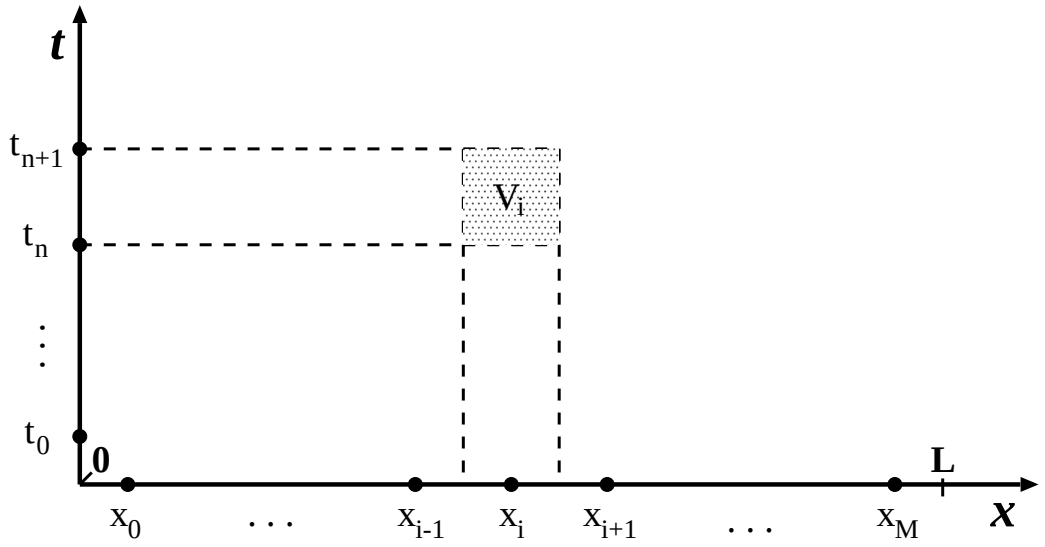

Figure 4.2: A control volume V_i in a space-time grid.

The choice of the parameter θ determines the type of time discretization. For $\theta = 0$ we have the Euler forward scheme, for $\theta = 1$ the scheme is Euler backward. The most common choice is $\theta = \frac{1}{2}$, which is the Crank-Nicholson scheme.

In general, the interior flux $q_{i-\frac{1}{2}}$ can be discretized by second order central differences as

$$q_{i-\frac{1}{2}} = -\kappa_{i-\frac{1}{2}} \frac{T_i - T_{i-1}}{x_i - x_{i-1}}, \quad i = 2, \ldots, M, \tag{4.30}$$

which represents the amount of heat flowing from V_{i-1} into V_i across a unit cross-sectional area per unit time. The discretization for $q_{i+\frac{1}{2}}$ is similar. The quantity $\kappa_{i-\frac{1}{2}}$, called the effective conductivity, is difficult to prescribe since in general the conductivities κ_{i-1} and κ_i can be different. By means of the so-called thermal resistance, given by

$$R_{i-\frac{1}{2}} = \frac{\frac{1}{2}\Delta x_{i-1}}{\kappa_{i-1}} + \frac{\frac{1}{2}\Delta x_i}{\kappa_i} \tag{4.31}$$

we can express the interior flux (4.30) as

$$q_{i-\frac{1}{2}} = -\frac{T_i - T_{i-1}}{R_{i-\frac{1}{2}}}, i = 2, \ldots, M. \tag{4.32}$$

As a convenient indicator of the state of phase of a control volume, the

liquid fraction defined as

$$\lambda_i^n = \begin{cases} 0, & \text{if } H_i^n \le 0 \quad \text{(solid)}. \\ \frac{H_i^n}{\rho L}, & \text{if } 0 < H_i^n < \rho L \quad \text{(mushy)}. \\ 1, & \text{if } \rho L \le H_i^n \quad \text{(liquid)}. \end{cases} \tag{4.33}$$

is often used. If $0 < \lambda_i^n < 1$ the control volume is said to be mushy with liquid volume $\lambda_i^n \Delta x_i$ and solid volume $(1 - \lambda_i^n)\Delta x_i$. If the problem admits a sharp interface, then according to [2], Chapter 4.2, the enthalpy scheme ought to produce a single mushy node at each time step. If at time t^n the mushy node is the m-th node, then a good approximation of the interface location $\Gamma^n(t^n)$ is given by

$$\Gamma^n := x_{m-\frac{1}{2}} + \lambda_m^n \Delta x_m. \tag{4.34}$$

We emphasize once again that the interface location itself is not involved in the computation at all, this being an essential advantage of the enthalpy method.

In addition, the liquid fraction can be used in choosing the effective conductivity κ_i of a mushy control volume, which can be quite difficult, especially in two or three spatial dimensions. For example, in case of a sharp front, one could choose κ_i^n using the relation

$$\frac{1}{\kappa_i^n} = \frac{\lambda_i^n}{\kappa_l(T_m)} + \frac{1 - \lambda_i^n}{\kappa_s(T_m)}, \quad i = 1, 2, \ldots, M. \tag{4.35}$$

Although many choices have been proposed in literature, the problems remains to decide which choice is most relevant to the problem considered.

For temperature dependent conductivities the best approach is to introduce the so-called Kirchoff temperature u defined as

$$u := \int_{T_m}^{T} \kappa(\tau) d\tau = \begin{cases} \int_{T_m}^{T} \kappa_s(\tau) d\tau & \text{for } T < T_m, \\ \int_{T_m}^{T} \kappa_l(\tau) d\tau & \text{for } T > T_m. \end{cases} \tag{4.36}$$

In particular, for constant κ_s, κ_l we have

$$u = \begin{cases} \kappa_s(T - T_m) & \text{if } T < T_m, \\ 0 & \text{if } T = T_m, \\ \kappa_l(T - T_m) & \text{if } T > T_m. \end{cases} \tag{4.37}$$

Then $q \equiv -\kappa T_x = -u_x$, so the discrete flux is simply $q_{i-\frac{1}{2}} = (u_{i-1} - u_i)/\Delta x$, and the discretized enthalpy equation reduces to

$$\frac{H_i^{n+1} - H_i^n}{\Delta t_n} = \frac{u_{i-1}^{n+\theta} - 2u_i^{n+\theta} + u_{i+1}^{n+\theta}}{\Delta x^2} + Q_i^{n+\theta}. \tag{4.38}$$

In [2], Chapter 4.3, it is even emphasized that, when the conductivities of the phases are unequal and they are functions of the temperature only and not of the location, the Kirchoff transformation should be used. One of the main reasons is that faster convergence can be obtained in case an implicit scheme is used, and thus efficiency is increased.

Difficulties also arise in case the heat capacities are temperature dependent. If $c_s = c_s(T), c_l = c_l(T)$ then in general we need to find T from an equation of the form (4.21), for which a Newton-Raphson method may be employed.

In case of $\theta = 0$ the fluxes are evaluated at the old time t^n and it is assumed that up to t^{n+1} the process is driven by these fluxes. This time-explicit scheme is very straight-forward, although there is one important restriction that needs to be addressed. To ensure stability the time step has to fulfill the well known Courant-Friedrichs-Lewy (CFL) condition, which in case of the enthalpy equation is given by

$$\Delta t^n \leq \frac{1}{2} \frac{(\min \Delta x)^2}{\max \alpha^n} \tag{4.39}$$

where $\min \Delta x = \min_{i=1,2,\ldots,M} \Delta x_i$ and

$$\max \alpha^n = \max_{i=1,2,\ldots,M} \left\{ \frac{\kappa_l(T_i^n)}{\rho c_i}, \frac{\kappa_s(T_i^n)}{\rho c_i} \right\}. \tag{4.40}$$

The advantage of a time-explicit scheme mainly lies is its simplicity and the ease with which is can be programmed.

For implicit schemes, where $\frac{1}{2} \leq \theta \leq 1$, there is no restriction to the choice of time step in order to ensure stability. But, because of the definition of the enthalpy as being dependent on temperature, we have a nonlinear system, which can only be solved using an iterative method. In fact, H_i as function of T_i is multi-valued when $T_i = T_m$, since it may be any number between 0 and ρL.

An often employed iterative method for linear systems is the Gauss-Seidel iteration. A standard method to accelerate the convergence of the Gauss-Seidel iteration is the successive over-relaxation (SOR) algorithm. Acceleration is obtained by linear extrapolation using an over-relaxation variable

ω. In general, convergence of the SOR-method is obtained for $0 < \omega < 2$. In case of $\omega = 1$ the SOR method is exactly the Gauss-Seidel method and acceleration is only achieved for $1 < \omega < 2$. For phase-change problems, and in particular the enthalpy problem as formulated above, which is highly nonlinear, Elliott and Ockendon have suggested a partial nonlinear SOR method which uses relaxation only when there is no phase-change [18]. Although both the standard and the Elliott-Ockendon SOR method are simple, writing out these schemes would be very elaborate and is therefore omitted. For a detailed description of the methods the reader is referred to [2, 18]. Furthermore, one could use the Newton-Raphson method which has the promise of up to quadratic convergence, whereas the nonlinear SOR can achieve at most linear convergence. Once again, we refer to [2], Chapter 4.3, for further details.

Extensive tests of the performance of the mentioned implicit schemes have been done of which the results are presented in [2], Chapter 4.3. The main conclusions are that

1. The implicit schemes are more advantageous for slow phase-change processes than for faster ones since for slow processes far larger time steps can be used.

2. Employing (Elliott-Ockendon) SOR with $1 < \omega < 2$ speeds up convergence considerably, while performance is poor when Gauss-Seidel iterations are used in solving the nonlinear system.

3. The Newton iteration scheme outperforms the SOR schemes, provided that the time step is not chosen too large.

Whether an explicit or implicit scheme is to be used relates strongly to the problem that is considered. Aspects that should be taken into consideration are among others the physical time scale, and not unimportantly the intended use. The larger the Stefan number (4.1), the faster the phase transition process and hence the smaller the time step must be for reasonable accuracy, which causes the implicit schemes to become less advantageous over the (time step size restricted) explicit ones. The intended use imposes restrictions on the choice of method in terms of computing effort, accuracy and ease of implementation. Implicit methods can become computationally demanding, especially when a higher order of accuracy is required. Besides, explicit methods are far more easy to implement.

It should be noted that the abrupt change in H as described by (4.22) gives rise to numerical difficulties. For instance, a naive discretization of the enthalpy equation on a uniform grid is well known to predict non-physical

features such as step-like movement of the phase boundary and spurious temperature plateaus [14]. When applying the Newton-Raphson method to solve the nonlinear system, determining the derivative of $u = T(H)$ in the Jacobian of the system gives rise to conceptual problems as to the the meaning and existence of this derivative, since the derivative experiences jumps at $H = 0$ and $H = \rho L$ [2], Chapter 4.3. Therefore, smoothing techniques and spreading of the phase-change temperature across a temperature interval need to be used, see for instance [15]. Smoothing can also be used to model materials that change phase over a temperature range rather than at a specified temperature. Nedjar [34] remarks that when regularization is used, as in [15], a possible deviation from the original problem may occur. Besides, it has been reported that smoothing of the enthalpy function on a stationary grid has to be done carefully, since the numerical results tend to become inaccurate when the amount of smoothing is too large. The accuracy can be improved by reducing the amount of smoothing, but this will eventually cause the step-like movement of the moving interface to reappear [42].

'Recent literature'

Fixed-grid enthalpy methods in combination with finite volume/finite difference discretizations are still quite popular. For instance Esen and Kutluay [19] have considered an enthalpy formulation to solve a one-dimensional one-phase problem with a Neumann-type boundary condition. Because of the many advantages, numerically speaking, the authors use a non-dimensional enthalpy formulation, given by:

$$\frac{\partial E}{\partial t} = \frac{\partial^2 U}{\partial x^2}, \tag{4.41}$$

where E, U are the non-dimensional enthalpy and temperature, respectively, to describe the heat flow. The (non-dimensional) temperature versus enthalpy relation within the liquid region is then given by

$$U = \begin{cases} E - \alpha, & E > \alpha \\ \\ 0, & 0 \leq E \leq \alpha \end{cases}, \tag{4.42}$$

where α is the Stefan number.

In order to avoid the well-known drawbacks of the explicit scheme (limited time step) or an implicit difference replacement (solution of a nonlinear system of algebraic equations), the odd-even Hopscotch algorithm is used. This method combines explicit and implicit finite difference replacements at

alternate mesh points in such a way that the overall scheme does not require the solution of a system of algebraic equations and as such it is overall explicit. Besides, the method is unconditionally stable. For more details, see [19].

The use of an enthalpy formulation is not restricted to fixed grids. Several methods have been developed for (adaptive) moving meshes. In order to incorporate the movement of the grid a semi-Lagrangian formulation is considered of the form:

$$\frac{\partial H}{\partial t} - \frac{dx}{dt}\frac{\partial H}{\partial x} = \frac{\partial^2 u}{\partial x^2} + Q, \tag{4.43}$$

where the Kirchoff transformation

$$u(T) = \int_{T_{ref}}^{T} \kappa(\zeta) d\zeta, \tag{4.44}$$

is used in order to allow for a temperature dependency of the thermal conductivity κ. Mackenzie and Robertson [30] employ a technique based on integrable monitor functions to generate appropriate grid point distributions as well as smoothing of the enthalpy function in order to obtain accurate results for the one-dimensional problems that they considered.

4.3.3 Finite element approaches

As has been remarked earlier, the enthalpy equation (4.20) is to be interpreted in a weak sense, due to the discontinuous derivatives of the enthalpy function H. In case a variational formulation is considered, these derivatives can be dealt with in a more natural way. The enthalpy problem on a domain Ω is given by:

$$H_t(T) - \nabla \cdot (\kappa(T)\nabla T) = Q(t), \tag{4.45}$$

subject to one or more of the following boundary conditions on the complementary parts $\delta\Omega_i, i = 1, 2, 3$ of the fixed outer boundary $\delta\Omega = \bigcup_{i=1}^{3} \delta\Omega_i$:

1. A Dirichlet condition on $\delta\Omega_1$:

$$T = \bar{T}_2(\boldsymbol{x}). \tag{4.46}$$

2. A Neumann condition on $\delta\Omega_2$:

$$\kappa(T)\frac{\partial T}{\partial \boldsymbol{n}}(\boldsymbol{x}) = \bar{q}(\boldsymbol{x}), \tag{4.47}$$

where $\mathbf{n}$ is the outward unit normal to the boundary surface, and $\bar{q}(\boldsymbol{x})$ a given normal heat flux.

3. A radiation-type boundary condition on $\delta\Omega_3$:

$$\kappa(T)\frac{\partial T}{\partial \boldsymbol{n}}(\boldsymbol{x}) = \bar{\alpha}(T), \tag{4.48}$$

where $\bar{\alpha}(T)$ is a non-linear function of temperature.

A variational formulation is obtained in a straightforward way. First we define a set $\mathbb{V}$ of test functions Ψ satisfying homogeneous boundary conditions on $\delta\Omega_1$ by

$$\mathbb{V} = \{\Psi \in H^1(\Omega) | \Psi = 0 \text{ on } \delta\Omega_1\}. \tag{4.49}$$

Next, we multiply equation (4.45) by an arbitrary test function $\Psi \in \mathbb{V}$, integrate of the domain Ω and apply the Gauss divergence theorem, which gives:

$$\begin{aligned}\int_\Omega \Psi H_t(T) d\Omega + \int_\Omega \nabla\Psi \cdot (\kappa(T)\nabla T) d\Omega - \int_\Omega \Psi Q d\Omega \\ - \int_{\delta\Omega_2} \Psi \bar{q}(T) d\Gamma - \int_{\delta\Omega_3} \Psi \bar{\alpha}(T) d\Gamma = 0.\end{aligned} \tag{4.50}$$

A finite difference scheme in time is used to resolve this problem numerically. In [34] the backward-Euler scheme is used, which results in a nonlinear system. To deal with the phase change, a relaxation of the increments of the enthalpy function as function of the actual temperature increments is used. The Galerkin finite element approximation is then applied to solve the resulting system at each time step iteratively for the two unknown quantities as two successive operations: first the temperature, which has to be treated as a continuous field ($T \in H^1(\Omega)$) on the nodal points, and secondly the enthalpy, which has to be treated as a discontinuous one ($H \in L^2(\Omega)$) on the quadrature points.

The presented method can be applied to mushy as well as isothermal problems. Although only one- and two dimensional examples are given in the article, the method is also applicable for three-dimensional phase-change problems.

Bhattacharya et al. [3] us a fixed-grid finite element based enthalpy formulation for phase-change problems in one-dimensional slabs of pure material. To deal with the isothermal phase-change, a superficial phase-change region is assumed around the discontinuity at the melting point.

The governing equation considered is a source free, energy balance equation:

$$\frac{\partial H}{\partial t} = \frac{\partial}{\partial x}\left(\kappa_{eff}\frac{\partial T}{\partial x}\right), \tag{4.51}$$

where $\kappa_{eff} = \phi_l \kappa_l + (1 - \phi_l)\kappa_s$ is the effective thermal conductivity and ϕ_l is the liquid volume fraction, which depends on the equilibrium phase diagram of the specific material involved, and is a function of temperature at a given position in the sample. Since ϕ_l is a step function in case of isothermal phase-change, a superficial phase-change range of ΔT around T_m is assumed, within which ϕ_l is assumed to vary linearly from 0 to 1. The following functional form for ϕ_l is used:

$$\phi_l = \begin{cases} 0 & T \leq T_I, \\ \frac{T - T_I}{T_F - T_I} & T_I \leq T \leq T_F \\ 1 & T \geq T_F \end{cases} . \tag{4.52}$$

Here $T_I = T_m - \Delta T/2$ is the initial melting point and $T_F = T_m + \Delta T/2$ is the final melting point. The enthalpy function of the system is written as:

$$H(T) = \rho(1 - \phi_l) \int_{T_{ref}}^{T} C_s d\tau + \rho \phi_l \left(\int_{T_{ref}}^{T_I} C_s d\tau + L + \int_{T_I}^{T} C_l d\tau \right). \tag{4.53}$$

Equation (4.51) is solved using the standard Galerkin finite element method for the single unknown variable T: the enthalpy function is rewritten in terms of the Galerkin approximation of the temperature using (4.53). For the time-derivative $\partial H/\partial t$ the unconditionally stable finite difference based Crank-Nicholson method is applied. The resulting system of nonlinear equations are solved at each time step using a Newton-Raphson procedure.

The position of the phase change front, $X = \Gamma(t)$, is computed by first locating the element which contains the melting point, T_m. The exact position of the front is then determined by interpolation of the basic functions using the finite element expansion,

$$T_m = \sum_{k=1}^{N} T_k \phi_k X, \tag{4.54}$$

where N is the number of elements.

4.3.4 Enthalpy related methods

Several methods have been proposed in the literature that show similarities with the enthalpy methods discussed in the previous sections. Most of these enthalpy related methods are discussed by Hu et al. [25]. They are the apparent capacity method, the effective capacity method, the heat integration

method and the source based method. These methods apparently tend to be quite inaccurate. The accuracy is in most cases strongly dependent on the time step. The only exception concerning the accuracy issue is the effective capacity method, but unfortunately this method is very troublesome to implement.

In a recent article, Chun and Park [13] present an enthalpy related fixed-grid method which is implicit in time. To deal with the nodal points across the solid-liquid interface a fictitious temperature concept is introduced. Assuming that the density across the phases is constant, the governing equations considered are:

$$\frac{\partial h}{\partial t} = \kappa \nabla^2 h \tag{4.55}$$

$$L v_n = \kappa_s \left.\frac{\partial h}{\partial n}\right|_s - \kappa_l \left.\frac{\partial h}{\partial n}\right|_l \tag{4.56}$$

Here, h is the sensible enthalpy (i.e. latent heat is not included in the enthalpy), n is the surface normal and v_n is the velocity of the phase front. Without loss of generality, the enthalpy at the melting temperature, h_m, is set to zero. Using fictitious enthalpies positioned at a grid distance Δx of the location of the phase front X, the following numerical discretization is derived:

$$\frac{h_i^{n+1} - h_i^n}{\Delta t} = \frac{\phi_{i+1}^{n+1} - 2\phi_i^{n+1} + \phi_{i-1}^{n+1}}{(\Delta x)^2} + S_i, \tag{4.57}$$

where

$$S_i = \frac{\xi L}{\Delta x}\frac{X^{n+1} - X^n}{\Delta t} \quad \text{for } |X^{n+1} - x_i| < \Delta x, \tag{4.58}$$

$$S_i = 0 \quad \text{for } |X^{n+1} - x_i| \geq \Delta x, \tag{4.59}$$

$$\xi = 1 - \frac{|X^{n+1} - x_i|}{\Delta x}, \tag{4.60}$$

$$\phi_i = \begin{cases} \kappa_l h_i & \text{for } h_i \geq h_m, \\ \kappa_s h_i & \text{for } h_i < h_m \end{cases}. \tag{4.61}$$

and x_i are the nodal points. The new position of the phase boundary is obtained from:

$$L\frac{X^{n+1} - X^n}{\Delta t} = \kappa_s \frac{h_m - [(1-\delta)h_{i-1}^{n+1} + L_i^{n+1}]}{\Delta x} - \kappa_l \frac{[(1-\delta)h_i^{n+1} + 1 + L_{i+2}^{n+1}] - h_m}{\Delta x}, \tag{4.62}$$

where $0 \leq \delta = |X^{n+1} - x_i| \leq 1$. Per time step, an iterative process is performed in which first the position of the boundary is updated using (4.62) and then equation (4.57) is solved until the phase boundary coordinate and enthalpy values are converged (for some convergence criteria).

The authors remark that the presented method yields no oscillations of the temperature and phase front, which are said to be commonly observed with the typical enthalpy method. The solution is oscillation-free since the phase boundary is treated as a line rather than a control volume. The method can be extended to two dimensional problems without much difficulty.

4.3.5 Some examples

Example 1
In order to show the importance of including the latent heat in the mark formation modeling, we consider the following artificial one-dimensional heat problem on a domain of unit length. Arbitrary units are assumed for all quantities involved. Initially, the temperature of the whole domain is equal to T_0. On both ends $x = 0, x = 1$, a simple Dirichlet boundary condition is imposed: $T(0) = T(1) = T_0 = 600$. The melting temperature $T_m = 660$, latent heat $L = 400$, specific heat $C = 1$ and conductivity $\kappa = 0.001$. Slightly off center in the domain we have an internal heat source, of width equal to half of the domain, at a uniform power level $Q = 12$. The heat source is active during the whole simulation from $t = 0$ to $t = 100$.

For these fixed parameters we numerically solve both the heat diffusion equation (3.2) ($v = 0$) and the enthalpy equation (4.20). We discretize the heat diffusion equation using second order central differences for the spatial derivative and the Euler forward scheme for the time integration. The enthalpy equation is discretized as (4.29) using (4.30) for the fluxes, which for constant κ, independent of x, T, simply reduces to a second order central difference scheme. By setting $\theta = 0$ we also have the Euler forward scheme for the time discretization.

In Figure 4.3 results are shown for a uniform grid in space and time. The number of nodes in x-direction $N = 21$. The number of time steps $M = 7500$. From the figures it can be concluded that the due to the inclusion of latent heat, the maximum temperature at $t = 100$ is, visibly lower than in case of plain heat conduction, as would be expected. Besides, the shape of the temperature profile for both cases does not differ much.

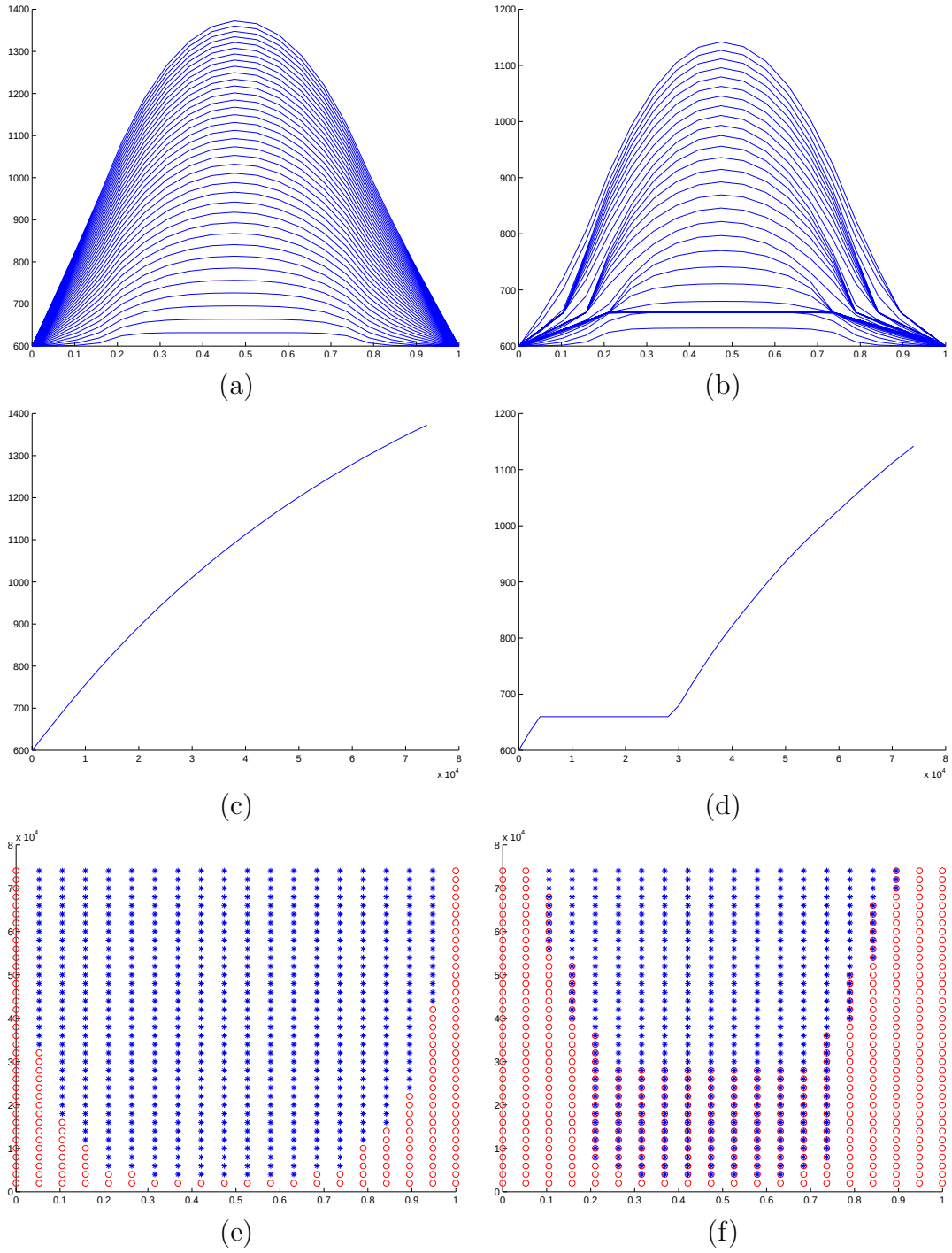

Figure 4.3: (a) T(x) without enthalpy, (b) T(x) with enthalpy, (c) T(t) of the central node without enthalpy, (d) T(t) of the central node with enthalpy, (e) phases with enthalpy, (f) phases without enthalpy. In figures (e) and (f) '*' represents liquid ($T > T_m$), 'o' represents solid ($T < T_m$) and where '*' and 'o' are overlapping, the material is at the melting temperature ($T = T_m$).

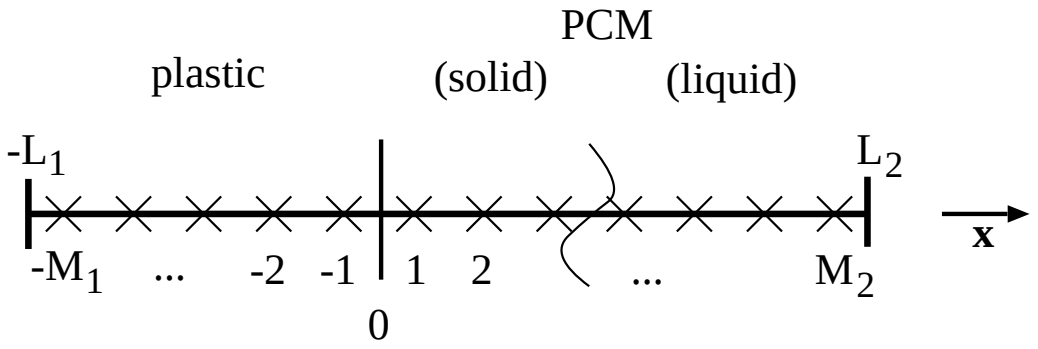

Figure 4.4: Spatial grid for a one-dimensional multi-layer consisting of a plastic and a phase-change material (PCM).

Example 2
As a second example we consider the use of the enthalpy method for a multi-layered slab. The problem described next has been taken from [2], Chapter 4.3, and involves a two-layered stack consisting of for instance a plastic and a hydrated salt (the phase-change material (PCM)), but the multi-layer might as well be the recording stack of an optical rewritable disk.

Let us consider a slab $-L_1 \leq x \leq L_2$ consisting of plastic: $-L_1 \leq x \leq 0$ and the PCM: $0 \leq x \leq L_2$. The region containing the plastic we subdivide into M_1 subintervals: $I_{-1}, I_{-2}, \cdots, I_{-M_1}$ of lengths $\Delta x_{-i}, i = 1, 2, 3, \cdots, M_1$, and the region containing the PCM into M_2 subintervals: $I_1, I_2, \cdots, I_{M_2}$ of lengths $\Delta x_i, i = 1, 2, 3, \cdots, M_2$. The discretization points x_j are defined as the midpoints of the intervals I_j for $j = -M_1, -M_1 + 1, \cdots, -1, 1, 2, \cdots, M_2$. See Figure 4.4

By taking the enthalpy to be dependent on location as well as temperature, the enthalpy method allows for treating the whole slab (i.e. plastic plus PCM) as one region. Of course, different thermo-physical properties of for the plastic, and the solid and liquid PCM should be used. The enthalpy $H(x,T)$ we define as:

$$H(x,T) = \begin{cases} \rho_p c_p (T - T_m), & -L_1 \leq x \leq 0, \\ \rho c_s (T - T_m), & 0 \leq x \leq L_2, \quad T < T_m \\ [0, \rho L], & 0 \leq x \leq L_2, \quad T = T_m \\ \rho L + \rho c_l (T - T_m), & 0 \leq x \leq L_2, \quad T > T_m \end{cases} \tag{4.63}$$

At position $x = 0$ we then have an 'interface' moving at zero speed, and

energy conservation across it will be ensured if the flux jump (by the Stefan condition) is zero there. Hence, the temperature T_0 at $x = 0$ can be determined form the equality of fluxes:

$$-\kappa_{-1}\frac{T_0 - T_{-1}}{\Delta x_{-1}/2} = -\kappa_1\frac{T_1 - T_0}{\Delta x_1/2}, \tag{4.64}$$

where κ_1 is κ_l or κ_s, depending on the phase of V_1. This yields

$$T_0 = \frac{\tilde{R}_1 T_{-1} + \tilde{R}_{-1} T_1}{\tilde{R}_{-1} + \tilde{R}_1}, \tag{4.65}$$

where $\tilde{R}_{-1} = \Delta x_{-1}/(2\kappa_{-1}), \tilde{R}_1 = \Delta x_1/(2\kappa_1)$, and the flux at $x = 0$ can be expressed as $q_0 = -(T_1 - T_{-1})/(\tilde{R}_{-1} + \tilde{R}_1)$, representing both $q_{-\frac{1}{2}}$ and $q_{\frac{1}{2}}$.

For the rest of the domain the enthalpy scheme is as described in Section 4.3.2. Thus, we update H_j from the global conservation law

$$H_j^{n+1} = H_j^{n+1} + \frac{\Delta t_n}{\Delta x_j}(q_{j-\frac{1}{2}}^{n+\theta} - q_{j+\frac{1}{2}}^{n+\theta}), \quad j = -M_1, \cdots, -1, 1, 2, \cdots, M_2, \tag{4.66}$$

and update T_j^{n+1} from

$$T_j^{n+1} = \begin{cases} T_m + \frac{H_j^{n+1}}{\rho_p c_p}, & j = -M_1, \cdots, -1 \\ T_m + \frac{H_j^{n+1}}{\rho c_s}, & j = 1, 2, \cdots, M_2, \quad \text{if } H_j^{n+1} < 0 \\ T_m, & j = 1, 2, \cdots, M_2, \quad \text{if } 0 \le H_j^{n+1} \le \rho L \\ T_m + \frac{H_j^{n+1} - \rho L}{\rho c_l}, & j = 1, 2, \cdots, M_2, \quad \text{if } H_j^{n+1} > \rho L. \end{cases} \tag{4.67}$$

The updated surface temperature at position $x = 0$ can be computed via (4.65):

$$T_0^{n+1} = \frac{\tilde{R}_1 T_{-1}^{n+1} + \tilde{R}_{-1} T_1^{n+1}}{\tilde{R}_{-1} + \tilde{R}_1}. \tag{4.68}$$

4.4 Level set methods

In the enthalpy method discussed in the previous section, the introduction of an enthalpy function that accounts for the latent heat absorption makes that the Stefan condition (3.6)

$$+\rho L v_n = \left[\kappa \frac{\partial T}{\partial \mathbf{n}}\right], \tag{4.69}$$

on the moving interface does not have to be enforced explicitly and therefore the front is only tracked implicitly. As we have seen, the method can be applied to both phase-change problems involving sharp fronts as well as problems with melting trajectories or mushy zones.

For Stefan problems in which the moving interface is sharp, level set approaches have been proposed. In the level set approach, the interface is represented by a signed distance function. This function $\phi(\mathbf{x}, t)$, appropriately called the level set function, is defined as:

$$\phi(\mathbf{x}, t) = \begin{cases} + \min\limits_{\bar{\mathbf{x}} \in \Gamma(t)} \|\mathbf{x} - \bar{\mathbf{x}}\| & \mathbf{x} \in \Omega_l, \\ 0 \quad \mathbf{x} \in \Gamma, \\ - \min\limits_{\bar{\mathbf{x}} \in \Gamma(t)} \|\mathbf{x} - \bar{\mathbf{x}}\| & \mathbf{x} \in \Omega_s. \end{cases} \tag{4.70}$$

The location of the moving boundary Γ is then equal to the zero level set of ϕ, i.e.:

$$\Gamma(t) = \{\mathbf{x} \in \Omega : \phi(\mathbf{x}, t) = 0\}. \tag{4.71}$$

The main idea of the level set method is to move ϕ with the correct speed, v_n, at the front and then to update the temperature, $T(\mathbf{x}, t)$, with the new position of the front stored implicitly in ϕ. When the new position of the front is known, updating the temperature comes down to solving the heat equation over the whole domain Ω, where special care has to be taken near the interface between the phases. We will return to this matter later.

The interface motion is governed by the conservation equation

$$\phi_t + F|\nabla\phi| = 0 \tag{4.72}$$

where F is a speed function that is a continuous extension of v_n off Γ onto all of Ω. The construction of F seems to be one of the most difficult aspects of the level set method, mostly since F highly depends on the phase-change problem considered, in particular the front velocity v_n and the number of spatial dimensions. For detailed examples on how to construct the speed function F see for instance [10], [11], [27].

The level set function ϕ can also be used to define the outward pointing normal $\mathbf{n}$ by

$$\mathbf{n} = \nabla\phi/|\nabla\phi| \tag{4.73}$$

and the interface curvature K by

$$K = \nabla \cdot \mathbf{n} = \nabla \cdot \left(\frac{\nabla\phi}{|\nabla\phi|} \right) \tag{4.74}$$

4.4.1 Numerical approaches

After its first introduction in 1988, the level set theory has been extensively developed, especially for finite difference methods, and has been employed to solve many different problems considering a sharp moving front. More recently, (extended/enriched) finite element methods (XFEM, [32]) are being proposed. Furthermore, hybrid methods, combining both XFEM and finite differences, have been developed [27].

An illustrative article on the application of a level set technique using finite differences for solving Stefan problems, is that of Chen et al. [10]. In order to capture the moving front on a fixed grid the method as described by the authors can be outlined as follows:

1. Initialize T and ϕ, so that ϕ is the signed distance from the interface.
2. Compute the extended velocity field F.
3. Update ϕ using equation (4.72) for one time step. The new position of the interface is then equal to the zero level set of ϕ. Since the level set function will cease to be an exact distance function, even after this one time step, a re-initialization of ϕ as described in [10] can be used to retain a distance function.
4. Away from the interface Γ solve the heat diffusion equation for T. For grid points less than or equal to a step size away from the front, appropriate numerical techniques are employed to approximate T.
5. Repeat steps 2 to 4 to get the next updated values of ϕ and T.

The numerical solving of the heat equation as mentioned in step 4 is not restricted to an implicit centered finite difference scheme, as proposed in the article, but can be any suitable discretization scheme. For details on the discretization of the velocity extension, discretization of the updating of the level set function, etc. the reader is referred to [10].

If a variational approach is considered, standard fixed grid based Galerkin approximations in which linear combinations of nodal shape functions are used, result in a continuous interpolation of for the temperature field. Furthermore, these approximation properties give rise to poor representations of arbitrary discontinuities. Therefore, standard finite element approaches require the employment of (adaptive) moving meshes and significant mesh refinements in order to resolve difficulties concerning these discontinuities and to properly deal with for instance moving heat sources.

The XFEM takes an alternative approach by extending the classical finite element approximation [32]. Let I be the set of all nodes in the mesh and J

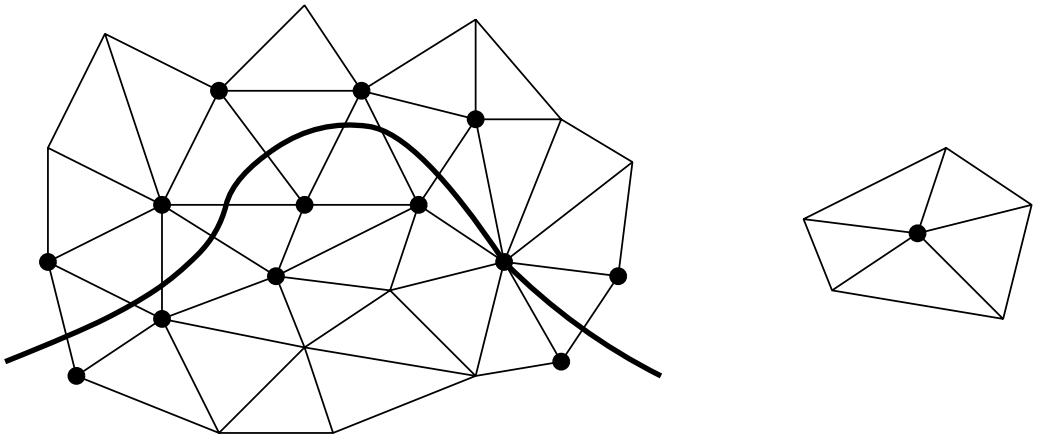

Figure 4.5: (a) The nodes that form a partition of unity for enrichment. (b) The support of a single nodal shape function.

the set of nodes that form a so-called partition of unity for the enrichment function $g(\mathbf{x})$, which we define as

$$J = \{j \in I |\ \omega_j \cap \Gamma \neq \emptyset\}, \tag{4.75}$$

where ω_j is the support of a single nodal shape function.

Then, in the XFEM, the temperature is given by

$$T(\mathbf{x}, t) = \sum_{i \in I} \phi_i(\mathbf{x}) T_i(t) + \sum_{j \in J} b_j \phi_j(\mathbf{x}) g(\mathbf{x}). \tag{4.76}$$

Thus, only those nodes are enriched, for which the front Γ crosses the support ω, as is illustrated in Figure 4.5. In practice, this means that for instance for triangular elements with three nodes, the enriched elements have six degrees of freedom, while the others have only three.

The key element of the XFEM is of course the enrichment function $g(\mathbf{x})$. Although in the case of phase-change problems, fairly little information is known about the local solution, at minimum a discontinuity in the temperature gradient normal to the interface can be expected. If we look at the classical approximation for the gradient of the temperature, given by

$$\nabla T(\mathbf{x}) = \sum_{i \in I} T_i \nabla \phi_i(\mathbf{x}), \tag{4.77}$$

where the ϕ_i are the standard $C^0(\Omega)$ shape functions, the above only contains jumps only across the element boundaries. This is exactly the motivation for

applying (adaptive) moving mesh techniques to match element boundaries to the phase interface.

In case of the XFEM approximation, the gradient is given by

$$\nabla T(\mathbf{x}) = \sum_{i \in I} T_i \nabla \phi_i(\mathbf{x}) + \sum_{j \in J} b_j (\nabla \phi_j(\mathbf{x}) g(\mathbf{x}) + \phi_j(\mathbf{x}) \nabla g(\mathbf{x})). \tag{4.78}$$

Arbitrary jumps in the gradient can thus be represented by a suitable choice of the function $g(\mathbf{x})$.

As is clearly illustrated by Merle and Dolbow [32], the influence of $g(\mathbf{x})$ on the accuracy can be high. A generally suitable choice $g(\mathbf{x}) = H(\|\mathbf{x} - \mathbf{X}\|)$, where H is the Heavyside function and X is the location of the moving front. To incorporate the level set function $\phi(\mathbf{x}, t)$, Chessa et al. [11] use

$$g(\mathbf{x}, \mathbf{t}) = |\phi(\mathbf{x}, t)| - |\phi_J(t)|, \tag{4.79}$$

where $\phi_J(t)$ are the nodal values of the level set field:

$$\phi_J(t) = \phi(\mathbf{x}_J, t). \tag{4.80}$$

The authors use a weak formulation to advect the level set field. Because the weak form of the motion equation (4.72) is a first order hyperbolic equation, stabilization is required to minimize oscillations in the numerical solution.

A far more complex construction of the partition of unity is studied by Ji et al. [27]. The authors investigate the use of $C^1(\Omega)$ continuous functions on a fixed rectangular grid. The enrichment of the finite element approximation is obtained by means of a projection onto the finite element grid. For further details on this hybrid method we refer to the article.

4.5 Method discussion and recommendation

The process of recording an amorphous mark during the writing of an optical disk is a problem involving melting and solidification. As has been explained in the previous Chapter, the formation of a mark can be modeled as a moving boundary problem. Or more precisely, as a two-phase Stefan problem. In this chapter a selection of numerical methods has been discussed to solve this Stefan problem, where we have mainly put emphasis on enthalpy and level set techniques.

We will now discuss the general benefits and drawbacks of the enthalpy and level set methods. Based on this overview a recommendation will be given concerning the most applicable numerical method to solve our melting

problem. As a guideline we will use the following list of requirements, of which most should be fulfilled by our method of choice.

List of requirements (in random order)

- Robust
- Simple
- Accurate
- Efficient
- Finite elements
- Three spatial dimensions
- Multidimensional (multiple separate fronts)
- Two or more phases
- Isothermal / non-isothermal (mushy)
- Equal and unequal thermal diffusivities etc.

The most important aspect with respect to the Stefan problem is of course how a numerical method deals with the moving front. Except maybe for the boundary conditions on the fixed boundaries, for all methods it holds that away from the moving front, the numerical techniques are mostly standard, since the problem is then reduced to solving the heat diffusion equation.

The enthalpy equation that arises from the enthalpy formulation, is quite similar to the heat conduction equation. The position of the moving boundary is implicitly incorporated in the enthalpy equation, and therefore no active tracking of the location of the front is required. Unfortunately, after discretizing the resulting system is highly nonlinear. Therefore, linearizations or advanced solvers for nonlinear systems have to be employed. The location of the boundary is determined as part of a post-processing step for which various techniques have been proposed with which fairly accurate results can be obtained. In general, the enthalpy methods perform best in case of non-isothermal problems. In case of isothermal problems a smoothing of the enthalpy equation is advisable in order to minimize oscillations. Due to the implicit description of the moving front, multiple fronts, kinks and the merging/separation of fronts can probably be dealt with, without much difficulty.

The explicit tracking of the moving front, such as with the level set method, is in particular interesting for problems in which the interface between phases is sharp. The location of the interface is accurately described by the zero level set of the level set function. Although the method essentially seems to be fairly simple and robust, there is one mayor disadvantage with respect to the level set function. In particular for phase-change problems, the construction of an extension of the velocity field to the whole domain can be very complicated, since only the velocity on the boundary itself is known. These difficulties increase with the number of spatial dimensions. Inclusion of the level set function as part of enhancement functions in XFEM or hybrid techniques in which advection of the level set function is performed using finite differences do not tackle this inherent difficulty.

Altogether it seems that the best approach for dealing with our melting problem is an enthalpy technique. Highly favorable are the simplicity of the governing equations (the Stefan condition is incorporated in the enthalpy equation) and the relatively easy extendibility to three spatial dimensions. Besides, positive aspects of the level set methods, such as being able to deal with irregular interfaces and merging fronts, can also be obtained with an enthalpy method. In particular the elaborate extension of the velocity field as required by the level set method.

Chapter 5

Test problems

Without a means of validating a numerical model, the model would essentially have no value. It is therefore that in this short chapter we will give an overview of a few test problems for which either a Neumann/similarity solution exists or for which strictly numerical results have been published. Each problem will only be described in short. For parameter values and other details we will refer to the appropriate articles.

One-dimensional two-phase melting/solidification problem

Consider a uniform finite half-space consisting of a solid material that is initially at temperature $T_I \neq T_m$, see Figure 5.1 (a). At $t = 0$ the temperature at the left edge is raised/lowered to a constant temperature $T_w \neq T_m$ which causes the slab to melt/solidify. The top and bottom edges are insulated. The exact solution to the corresponding uniform semi-infinite half-space melting problem is given by Neumann's solution, see Subsection 4.1.1.

Bhattacharya et al. [3] resolve this type of problem using a standard Galerkin finite element method. In their enthalpy formulation the authors assume a superficial phange change range of width ΔT around T_m. A linear enthalpy versus temperature relation is assumed in this range.

A similar problem is studied by Chun and Park [13]. They employ an enthalpy related fixed-grid finite-difference method. The authors compare their results not only with the similarity solution, but also with several methods as published by other authors. Results are presented for both equal or unequal diffusivities.

Infinite corner solidification problem

A second example taken from [11] considers the corner of an infinite quarter-space of fluid which has an initial temperature $T_{in} > T_m$, see Figure 5.1 (b).

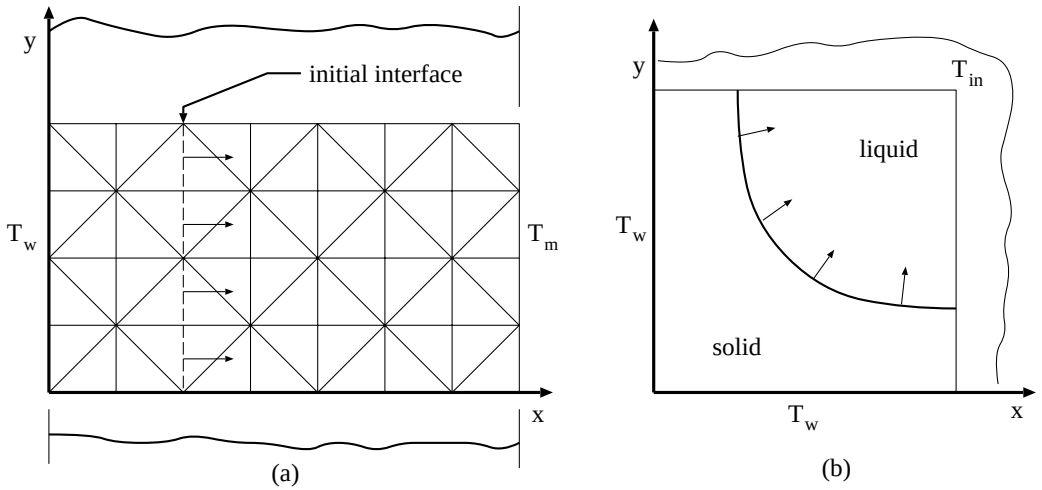

Figure 5.1: (a) A one-dimensional melting problem for a finite slab and (b) an internal corner solidification problem with an interface shown for $t > t_0$.

At time $t > t_0$ a constant temperature $T_w < T_m$ is applied to the exterior walls. This causes the quarter-space to solidify. In case the diffusivities of both phases are equal, an analytical solution exists. For more details on the similarity solution to this problem, we refer to [11].

Square solidification problem

This problem is essential the same as the previous example, except that in this case we consider a finite square domain. Initially the square domain consists of a material in the liquid state at the melting temperature. At time $t = 0$ the temperature at the fixed boundaries is lowered to $T_w < T_m$ which inititiate an inwards solidification process. In Figure 5.2 the problem configuration is shown at a time $t > 0$. A selection of references to authors that have numerically solved this problem can be found in [11].

Unfortunately, so far no test problems containing an internal source have been found in the literature.

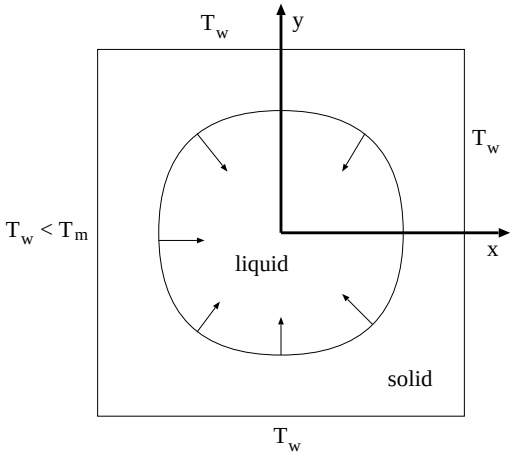

Figure 5.2: The problem configuration for the square solidification problem.

Bibliography

[1] *Proceedings ISOM*, 2000.

[2] V. Alexiades and A.D. Solomon. *Mathematical modeling of melting and freezing processes*. Hemisphere Publishing Corporation, 1993.

[3] M. Bhattacharya, T. Basak, and K.G. Ayappa. a fixed-grid finite element based enthalpy formulation for generalized phase change problems: Role of superficial mushy region. *Int. J. Heat and Mass Transf.*, 45:4881–4898, 2002.

[4] *Proc. SPIE*, volume 191, 1999.

[5] H.J. Borg, M. van Schijndel, J.C.N. Rijpers, M. Lankhorst, G. Zhou, M.J. Dekkers, I.P.D. Ubbens, and M. Kuijper. Phase-change media for high-numerical-aperture and blue-wavelength recording. *Jpn. J. Appl. Phys. Part 1*, 40:1592–1597, 2001.

[6] J.M. Brok and H.P. Urbach. Rigorous model of the scattering of a focused spot by a grating and its application in optical recording. *J. Opt. Soc. Am. A*, 20(2):256–272, 2003.

[7] J.H. Brusche. The integration of an optical and a thermal model for applications in optical recording. internal report, Philips Research Laboratories, Eindhoven, the Netherlands, 2002.

[8] L. Cheng C. Peng and M. Mansuripur. Experimental and theoretical investigations of laser-induced crystallization and amorphization in phase-change optical recording media. *J. Appl. Phys.*, 82(9):4183–4191, 1997.

[9] J. Carriere, R. Narayan, W. Yeh, C. Peng, P. Khulbe, L. Li, R. Anderson, J. Choi, and M. Mansuripur. Principles of optical disk storage. In E. Wolf, editor, *Progress in optics*, volume 40. Elsevier Science B.V., 2000.

[10] S. Chen, B. Merriman, S. Osher, and P. Smereka. A simple level set method for solving Stefan problems. *J. Comp. Ph.*, 135:8–29, 1997.

[11] J. Chessa, P. Smolinski, and T. Belytschko. The extended finite element method (XFEM) for solidification problems. *Int. J. Numer. Meth. Engng.*, 53:1959–1977, 2002.

[12] D.M. Christopher. Comparison of interface-following techniques for numerical analysis of phase-change problems. *Num. Heat Transf., Part B*, 39:189–206, 2001.

[13] C.K. Chun and S.O. Park. A fixed-grid finite-difference method for phase-change problems. *Num. Heat Transf., Part B*, 38:59–73, 2000.

[14] J. Crank. *Free and moving boundary problem*. Clarendon Press, Oxford, 1984.

[15] A.J. Dalhuijsen and A. Segal. Comparison of finite element techniques for solidification problems. *Int. J. Numer. Meth. Engng.*, 23:1807–1829, 1986.

[16] S.H. Davis. *Theory of solidification*. Cambridge University Press, New York, 2001.

[17] J.P.W.B. Duchateau and B.A.J. Jacobs. Phase-change recording. internal report M.S. 18.901, Philips Research Laboratories, Eindhoven, the Netherlands, 2001.

[18] C.M. Elliott and J.R. Ockendon. *Weak and variational methods for moving boundary problems*. Pitman Press, Boston, 1982.

[19] A. Esen and S. Kutlay. A numerical solution of the Stefan problem with a Neumann-type boundary condition by enthalpy method. *Appl. Math. Comput.*, 148:321–329, 2004.

[20] Z. Fan and D.E. Laughin. Three dimensional crystallization simulation and recording layer thickness effect in phase change optical recording. *Jpn. J. Appl. Phys.*, 42(2B):1–4, 2002.

[21] R.P. Feynman, R.B. Leighton, and M. Sands. *The Feynman lectures on physics. Vol. 2. Mainly electromagnetics and matter*. Addison-Wesley, Reading, 1977.

[22] J.W. Goodman. *Introduction to Fourier optics*. McGraw-Hill, New York, second edition, 1998.

[23] S.C. Gupta. A moving grid numerical scheme for multi-dimensional solidification with transition temperature range. *Comput. Methods Appl. Mech. Engrg.*, 189:525–544, 2000.

[24] Gibbs free energy. *http://xenon.che.ilstu.edu/genchemhelphomepage/topicreview/bp/ch21/gibbs.html*.

[25] H. Hu and S.A. Argyropoulos. Mathematical modelling of solidification and melting: A review. *Modelling Simul. Mater. Sci. Eng.*, 4:371–396, 1996.

[26] H. Iwasaki, M. Harigaya, O. Nonoyama, Y. Kageyama, M. Takahashi, K. Yamada, H. Deguchi, and Y. Ide. Completely erasable phase change optical disc II: Application of Ag-In-Sb-Te mixed-phase system for rewritable compact disc compatible with CD-velocity and double CD-velocity. *Jpn. J. Appl. Phys.*, 32B:5241–5247, 1993.

[27] H. Ji, D. Chopp, and J.E. Dolbow. A hybrid extended finite element/level set method for modeling phase transformations. *Int. J. Numer. Meth. Engnh.*, 54:1209 – 1233, 2002.

[28] J.B. Judkins and R.W. Ziolkowski. Finite-difference time-domain modeling of nonperfectly conducting metallic thin-film gratings. *Appl. Opt.*, 12:1974–1983, 1995.

[29] W.-C. Liu and M.W. Kowarz. Vector diffraction from subwavelength optical disk structures: two-dimensional modeling of near-field profiles, far-field intensities, and detector signals from a DVD. *Appl. Opt.*, 38:3787–3797, 1999.

[30] J.A. Mackenzie and M.L. Robertson. The numerical solution of one-dimensional phase change problems using an adaptive moving mesh method. *J. Comp. Phys.*, 161:537–557, 2000.

[31] D.S. Marx and D. Psaltis. Optical diffraction and focused spots and subwavelength structures. *J. Opt. Soc. Am. A*, 14:1268–1278, 1997.

[32] R. Merle and J. Dolbow. Solving thermal and phase change problems with the eXtended finite element method. *Comp. Mech.*, 28:339–350, 2002.

[33] N. Miyagawa, Y. Gotoh, E. Ohno, K. Nishiuchi, and N. Akahira. Land and groove recording for high track density on phase-change optical disks. *Jpn. J. Appl. Phys. Part 1*, 38(11B):5324–5328, 1993.

[34] B. Nedjar. An enthalpy-based finite element method for nonlinear heat problems involving phase change. *Computers and Structures*, 80:9–21, 2002.

[35] Y. Nishi, T. Shimano, H. Kando, M. Terao, and T. Maeda. Simulations of marks formed on phase-change, land/groove disks. *Jpn. J. Appl. Phys.*, 41:2931–2938, 2002.

[36] C. Peng and M. Mansuripur. Thermal cross-track cross talk in phase-change optical disk data storage. *J. Appl. Phys.*, 88(3):1214–1220, 2000.

[37] D.J. Safarik and C.B. Mullins. Surface phase transformation kinetics: A geometrical model for thin films of nonvolatile and volatile solids. *J. Chem. Phys.*, 117(17), 2002.

[38] S. Senkader and C.D. Wright. Models for phase-change of $Ge_2Sb_2Te_5$ in optical and electrical memory devices. *J. Appl. Phys.*, 95(2):504–511, 2004.

[39] J. Stefan. Uber die Theorie der Eisbildung, insbesondere uber die Eisbildung im Palarmeere, Wien. *Akad. Mat. Naturw.*, 98(11a):965–983, 1889.

[40] W.A. van Helden. Phase change optical recording, a literature survey. company restricted, Philips Electronics, 1999.

[41] *Proceedings Optical Data Storage*, 1998.

[42] D.G. Wilson and P.T. Boggs, editors. *Moving boundary problems*, page 165. Academic Press, San Diego, 1978.

[43] E.M. Wright, P.K. Khulbe, and M. Mansuripur. Dynamic theory of crystallization in $Ge_2Sb_{2.3}Te_5$ phase-change optical recording media. *Appl. Opt.*, 39(35):6695–6701, 2000.

[44] N. Yamada, E. Ohno, K. Nishiuchi, and N. Akahira. Rapid-phase transitions of Ge-Te-Sb_2-Te_3 pseudobinary amorphous thin-films for an optical disc memory. *J. Appl. Phys.*, 69(5):2849–2856, 1991.

[45] W.-H. Yeh, L. Li, and M. Mansuripur. Vector diffraction and polarization effects in optical disk systems. *Appl. Opt.*, 37:6983–6988, 1998.